Title: *Aspergillus* dsRNA virus drives fungal fitness and pathogenicity in the mammalian host

Authors list: Vanda Lerer*[1], Marina Rocha*[1], John Adeoye*[1], Hilla Hayby[1], Neta Shlezinger[1]

Affiliations: [1] Koret School of Veterinary Medicine, Faculty of Agriculture, The Hebrew University, Rehovot, Israel

Corresponding author: neta.shlezinger1@mail.huji.ac.il

Keywords: mycovirus, hypervirulence, polymycovirus, *Aspergillus fumigatus*, viability, host-pathogen interaction

*Equally contributed

ABSTRACT

Fungal pathogens pose a significant threat to global health. *Aspergillus fumigatus* accounts for approximately 65% of all invasive fungal infections in humans, with mortality rates from aspergillosis reaching nearly 50%. Fungal virulence in plant pathogenic fungi can be modified by mycoviruses, viruses that infect fungi. However, their impact on fungal pathogenesis in mammals has remained largely unexplored. Here, utilizing an *A. fumigatus* strain naturally infected with Aspergillus fumigatus polymycovirus-*1M* (AfuPmV-1M), we found that the mycovirus confers a significant survival advantage to the fungus under conditions of oxidative stress, heat stress, and within the murine lung. Thus, AfuPmV-1M modulates fungal fitness, resulting in increased virulence and the progression of exacerbated fungal disease. Moreover, antiviral treatment reverses the exacerbated virus-mediated virulence, representing a promising "antipathogenicity" therapy against virus-bearing pathogenic fungi. Taken together, these data suggest that mycoviruses play a significant role as "backseat drivers" in human fungal diseases, presenting critical clinical implications.

Main Text

Human fungal pathogens contribute to a significant annual global burden, resulting in an estimated 1 billion infections and over 1.6 million deaths. This mortality rate is comparable to tuberculosis and surpasses that of malaria and breast cancer[1]. Mortality rates from invasive fungal infections (IFI) currently stand at approximately 50%, even with standard care. Furthermore, epidemiologists anticipate a consistent rise in IFI cases due to the growing population of individuals with compromised immune systems[2]. Pathogenic filamentous fungi are commonly found in soil and have a ubiquitous presence. These fungi produce a substantial quantity of conidia, which are then released into the air and dispersed by wind. When inhaled, these conidia have the ability to penetrate the respiratory tract [3]. In individuals with a competent immune system, the conidia are efficiently eliminated from the lungs. However, immunocompromised patients face a heightened risk of developing acute invasive mycosis. Among all invasive fungal infections in humans, *Aspergillus fumigatus* (*A. fumigatus*) constitutes approximately 65% of the cases, and the mortality rates for disseminated disease can reach up to 50% [2].

While fungi play a significant role in causing diseases in humans, animals, and plants, they are not immune to viral infections. Mycoviruses, viruses that infect fungi, are pervasive in the fungal kingdom, infecting over 20% of the tested isolates [4].
The overwhelming majority of mycoviruses possess either double-stranded (ds) or single-stranded (ss) RNA genomes, with only one family known to have circular ssDNA genomes [4]. While certain mycoviral infections exhibit benign characteristics, there are notable instances where mycoviruses have either advantageous or detrimental impacts on their fungal hosts. These effects encompass a range of outcomes, including modified virulence [5,6], drug resistance [7], mycotoxin production [8,9], and enhanced thermotolerance [10]. However, the molecular mechanisms governing mycoviral replication and their consequences on their fungal hosts remain inadequately understood. This is particularly true for the intricate interplay among mycoviruses infecting human pathogenic fungi, the fungal host itself, and the mammalian host.

The Af293 strain of *A. fumigatus* naturally harbors Aspergillus fumigatus polymycovirus-1 (AfuPmV-1M), a segmented dsRNA virus with four ORFs, belonging to the *Polymycoviridae* family [11]. Subsequent investigations revealed the existence of a closely related variant, AfuPmV-1M, which encodes a fifth ORF with no known annotation [12]. The significance of

these mycoviruses in aspergillosis remains a topic of limited exploration, with only two studies presenting contrasting phenotypic outcomes. One study suggests virus-induced hypervirulence in a *Galleria mellonella* infection model[11], while another indicates virus-induced hypovirulence in an immunosuppressed model of invasive aspergillosis[12]. Furthermore, recent studies have reported modified fungal virulence and the modulation of the mammalian immune response by mycovirus-bearing clinical isolates of *Talaromyces* and *Malassezia* [6,13,14]. These findings suggest that mycoviral infections contribute to fungal strain-specific virulence and host adaptation.

However, the underlying mechanisms that govern mycovirus-mediated fungal virulence and disease outcomes during mammalian infection remain unclear and necessitate further investigation. Here, we sought to assess how mycoviral infection affects *A. fumigatus* fitness, virulence, and the infection outcome.

Results

AfuPmV-1M Modulates Conidiation in *A. fumigatus*

To investigate the consequences of mycoviral infections on *A. fumigatus* physiology, we initially determined the specific polymycovirus variant present in our Af293 laboratory strain (Fig. 1). We performed agarose gel electrophoresis on dsRNA extracted from Af293 cells, which resulted in the resolution of four distinct bands, corresponding to ORF1-4 of AfuPmV-1M (Fig 1a). Notably, ORF 4 and ORF 5 share a similar size of approximately 1150 bp (1140 bp and 1158 bp, respectively), making them indistinguishable using agarose gel alone. To determine if the identified virus encodes ORF5, we conducted reverse transcription PCR analysis on both total RNA and isolated viral particles (Fig. 1b). This analysis confirmed the presence of ORF1-5, providing evidence for the presence of the AfuPmV-1M variant. To generate a congenic virus-cured (VC) strain, we utilized the cycloheximide translation inhibition curing approach[15]. Subsequently, the virus was reintroduced into the VC strain to generate a re-infected strain (RI) through protoplast transfection with AfuPmV-1M dsRNA [11]. The purity of the decontaminated strain (VC) and successful reintroduction of ORF1-5 were verified through reverse transcription PCR and quantitative real-time PCR analysis of total RNA (Fig. 1c-d). To confirm that the observed phenotypes are AfuPmV-1M-specific and that the cycloheximide treatment did not lead to detrimental genetic changes, we have generated an additional cured strain using the antiviral nucleoside analog Ribavirin, as previously described[16] (Supplementary Fig. 1a). Additionally, we generated whole-genome Illumina data and then performed genome-wide analyses and single nucleotide polymorphism

(SNP) calling of the *A. fumigatus* cycloheximide-cured, ribavirin-cured, and re-infected strains, comparing it to the virus-infected ancestral strain Af293. No nucleotide-changes were identified in the derivative strains and no substantial changes in ploidy or aneuploidy were observed for any chromosome (Supplementary Fig. 1b).

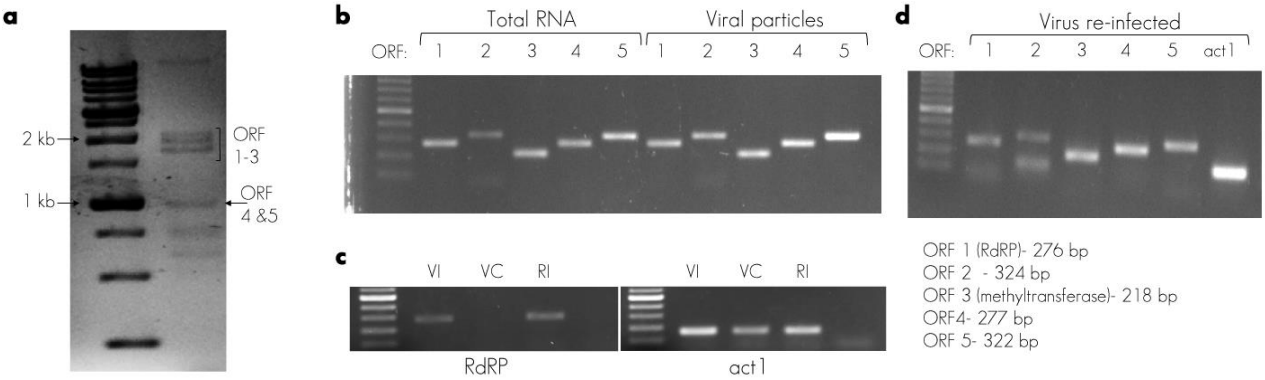

Figure 1. Identification of Afumpv-1M and generation of congenic virus-cured and re-infected strains. a. dsRNA extracted from *A. fumigatus Af293* and treated with DNase I and S1 nuclease was fractionated on a 1% agarose gel. **b.** Reverse-transcription PCR amplification to confirm the presence of *AfuPmV-1M* ORF 1-5 in Af293 total RNA and isolated viral particles. **c.** Reverse-transcription PCR (RT-PCR) amplification of a 276 bp segment from Afupmv-1M RdRP in total RNA extracted from Af293 (VI), cycloheximide virus-cured (VC), and Re-infected (RI) strains. **d.** RT-PCR amplification of *AfuPmV-1M* ORF 1-5 from total RNA extracted from the re-infected strain.

In agreement with previous studies[11], the three congenic strains displayed comparable radial growth, biomass production, biofilm formation, and germination rates (Supplementary Fig. 2). However, both the original virus-infected (VI) and re-infected (RI) strains exhibited colonies with a darker color, suggesting an elevation in conidiation and/or melanin production when compared to the virus-cured (VC) strains (Fig. 2a, Supplementary Fig. 3a). Indeed, the quantitative analysis of conidia number per plate and per conidiophore demonstrated a significant decrease in asexual conidia production in the virus-cured strains (Fig. 2b-d, Supplementary Fig. 3b). Moreover, besides the altered conidiation, the expression of genes involved in DHN-melanin biosynthesis was found to be upregulated in the virus-infected strains, establishing a clear relationship between the expression of DHN-melanin biosynthesis genes and the presence of AfuPmV-1M (Fig. 2e).

AfuPmV-1M Enhances Survival During Sporulation and Environmental Stresses

Infection by pathogenic fungi requires fungal survival within and escape from the leukocyte phagosome, an extremely inhospitable environment. This includes reactive oxygen species, low pH, and elevated temperature. Therefore, we compared the susceptibility of the virus-infected and virus-cured strains to a variety of stress conditions (Fig. 3).

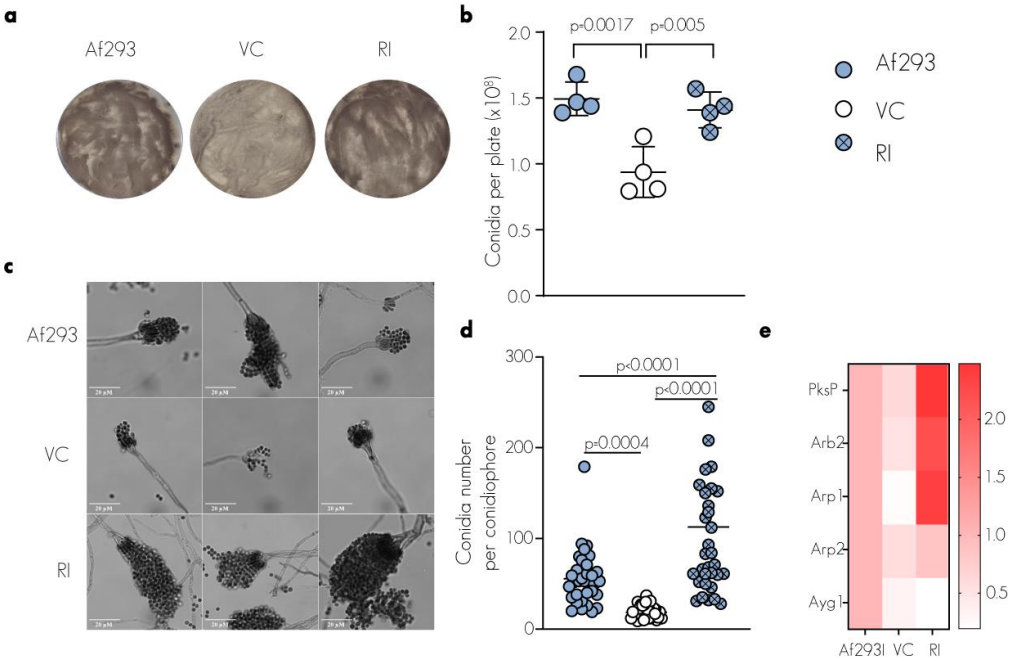

Figure 2. AfuPmV-1M regulation of conidiation and melanin production. a. AfuPmV-1M-infected strains (Af293 and RI) exhibit darker colonies compared to the cycloheximide virus-cured strain. 2×10^5 conidia (CFUs) were spread over GMM plates and grown for 7 days. **b.** Quantification of conidia number per plate. **c.** Representative micrographs of conidiophores. **d.** Conidia number per conidiophore. **e.** Relative expression of the *A. fumigatus* gene cluster involved in DHN-melanin biosynthesis. Data are derived from four biologically independent experiments. Statistical analysis: (**b,d**) one-way ANOVA with Tukey's multiple comparison test. Conidial suspensions were adjusted based on viability staining to account for differences in conidial viability prior to each experiment.

The three strains exhibited similar growth rates and survival in the presence of the cell wall–targeting antifungal drug voriconazole, as well as under conditions of both low and high pH, and osmotic stress (Supplementary Fig. 2&3). However, a comparative analysis of conidial viability during conidiation on plates revealed enhanced viability of newly formed conidia within colonies of the virus-infected strains compared to the virus-cured strain (Fig. 3a, Supplementary Fig. 3c-d). Moreover, the virus-infected strains showed heightened resistance to oxidative challenges and elevated temperatures, whereas the virus-cured strains displayed increased conidiation under these conditions (Fig. 3b-e, Supplementary Fig. 3e-o). Remarkedly, mycoviral transcription was upregulated under these conditions as asses by RT-qPCR of ORF1-5 during conidiation, under oxidative stress and heat shock, and during infection in a murine pulmonary invasive aspergillosis model (Fig. 3f-i).

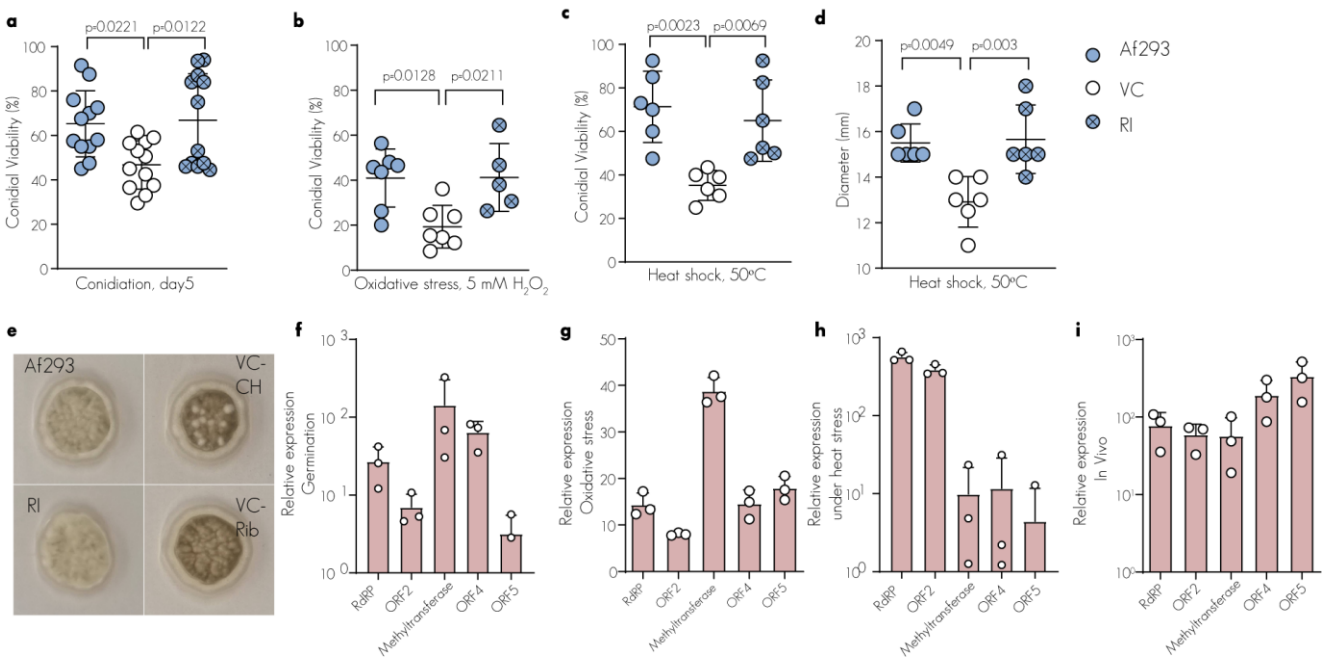

Figure 3. Afupmv-1M Mediates Cytoprotective Response to Environmental Stresses. a. Conidial viability during conidiation. 2×10^5 *Af293*, cycloheximide virus-cured (VC) and virus-re-infected (RI) conidia (CFUs) were spread on GMM plates and grown for 5 days. Conidia were then harvested, stained with propidium iodide, and analyzed by flow cytometry. **b-c.** Swollen conidia (4 h) were exposed to 5 mM H_2O_2 (**b**) or 50°C (**c**) for additional 4 h and analyzed for CFUs. **d-e.** 2×10^5 conidia (CFUs) were spread over GMM plates and grown for 3 days at 50°C. **d.** Radial growth. **e.** AfuPmV-1M cycloheximide-cured (VC-CH) and Ribavirin-cured (VC-Rib) strains exhibit increased conidiation under heat stress compared to Afupmv-1M-infected strains. For all stress assays, GMM at 37°C was used as control. **f-i.** Real-time qPCR showing relative expression levels of AfuPmV-1M ORF 1-5 during conidiation (day 3, **f**), upon oxidative stress (5 mM, 4h, **g**), heat shock (50°C, 4 h, **h**), and in vivo in IA model (24 h p.i., **i**). Statistical analysis: (**a**-**d**) one-way ANOVA with Tukey's multiple comparison test. Conidial suspensions were adjusted based on viability staining to account for differences in conidial viability prior to each experiment.

To elucidate the underlying mechanism through which AfuPmV-1M influences fungal fitness, we conducted a comprehensive investigation of global virus-derived proteomic alterations under both physiological conditions and oxidative stress, employing proteomic profiling (Fig. 4 and Table 1, Dataset 1). In this analysis, we quantified a total of 3,390 to 3,525 proteins. To ensure precision, we applied stringent criteria (a >2-fold change with a p-value <0.05) to filter the data and identify proteins that exhibited differential regulation in a virus-dependent manner. Our findings revealed that under physiological conditions, the AfuPmV-1M-infected strain Af293 displayed significant alterations in protein expression compared to the congenic virus-cured strain. Specifically, we observed upregulation of 19

proteins and downregulation of 6 proteins in the AfuPmV-1M-infected strain under control conditions. The most upregulated protein in the presence of AfuPmV-1M is Brf1 (Afua3g12730), a subunit of transcription factor TFIIIB complex required for accurate initiation of transcription by RNA Polymerase III (Pol III), which synthesizes transfer RNAs (tRNAs), 5S ribosomal RNA (rRNA), and other essential RNA molecules [17]. To validate this result, we conducted RT-qPCR to quantify the expression of Brf1 and selected TFIIIB gene targets (Fig. 4c). The Pol III genes analyzed included U6 snRNA (U6), tRNA-Arg (Arg), tRNA-Phe (Phe), and tRNA-Tyr (Tyr). Consistent with the proteome data, we observed that under physiological conditions, the expression levels of Brf1, U6, Arg, and Tyr were higher in Af293 and the re-infected strains compared to the virus-cured strain.

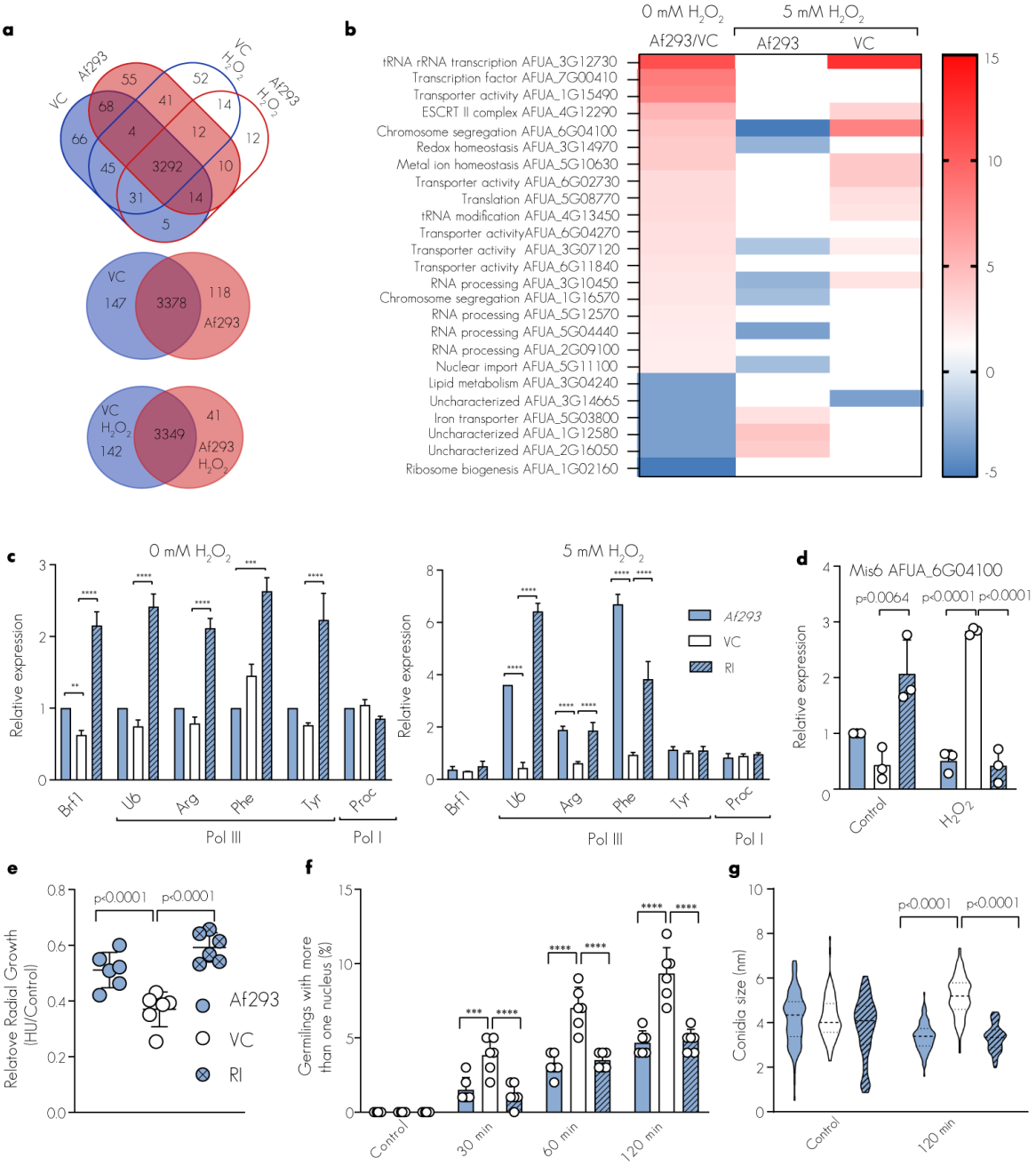

Figure 4. The proteome of AfuPmV-1M-infected *A. fumigatus* is altered. The protein content of *A. fumigatus* Af293 and cycloheximide virus-cured (VC) was characterized using mass spectrometry (MS) under physiological and oxidative stress conditions. **a.** The distribution of the identified proteins by their presence/absence. Only proteins that appeared in 3 out of 3 triplicates (n = 3) from each group were included in the final list. **b.** A total of 117 proteins were differentially abundant across the strains and growth conditions, based on an uncorrected value of <0.05 by analysis of variance (ANOVA). **c.** Relative mRNA levels in Af293 versus *VC* and *RI* under control conditions and upon oxidative challenge (5 Mm H_2O_2, 4h) analyzed by qRT-PCR. Analyzed genes: Brf1, Pol III-transcribed genes: U6 snRNA (U6), tRNA-Arg (Arg), tRNA-Phe (Phe), and tRNA-Tyr (Tyr), Pol I-transcribed procyclin (Proc). Data are mean + s.e.m., n = 3. ** = 0.0085,***= 0.0002 , **** <0.0001. **d.** Relative Mis6 levels in Af293 versus *VC* and *RI* under control conditions and upon oxidative challenge (5 Mm H_2O_2, 4h), analyzed by qRT-PCR. Data are mean + s.e.m, n = 3. **e.** Growth inhibition after 5 days on solid GMM media with 10 mM hydroxyurea. GMM at 37°C was used as a control**. f-g.** Mitosis Assay. Conidia were grown for 5 hours at 37°C in complete medium (YG) + 100 mM hydroxyurea, then washed and incubated again in YG medium for the indicated periods of time. The number of nuclei in each conidium (**f**) and conidial diameter (**g**) were assessed by Hoechst staining and light microscopy (50 germlings were counted per each repetition, the average of three independent experiments ± SD). **** <0.0001. Conidial suspensions were adjusted based on viability staining to account for differences in conidial viability prior to each experiment.

Table 1- Selected proteins altered in AfuPmV-1M+ proteomes. Protein content of the AfuPmV-1M-infected and cycloheximide-cured strains was catalogued by mass spectrometry. Data are mean + s.e.m., n=3. The full proteomic analyses can be consulted in supplemental data files (Dataset 1).

When subjected to oxidative stress, Brf1 expression remained unchanged, in line with the proteome data, while its targets U6, Arg, and Phe increased. Importantly, procyclin, a Pol I-transcribed gene, remained unaffected by the presence of the virus, indicating that AfuPmV-1M specifically regulates the transcription of Pol III targets. Interestingly, Brf1 and the products of its target genes have been shown to localize within stress granules (SGs). These dynamic cytoplasmic condensates rapidly form during various stress conditions, including heat shock, oxidative stress, hypoxia, bacterial, and viral infections [18–20]. These complexes store translational preinitiation complexes and can be rapidly released to resume gene expression when cellular stress conditions subside. Moreover, our proteomic analysis has identified additional known components of SGs that exhibit an AfuPmV-1M-dependent upregulation. These components include Ribosomal protein L24E (Afu5g08770), RNA methyltransferase (Afua4g13450), RNA polymerase III subunit C11 (Afua1g06380), U6 small nuclear ribonucleoprotein (Lsm3) (Afua5g12570), Thioredoxin (Afua3g14970), RNase III (Afua5g04440), and polyadenylation factor subunit CstF64 (Afua2g09100) (Fig. 4b) [21,21–26]. The formation of SGs has been demonstrated to play a pivotal role in driving stress adaptation and promoting cell survival[27]. Therefore, our findings, which demonstrate that AfuPmV-1M-infected strains show increased resistance to oxidative and heat stress, along with the observation that components of SGs are upregulated in the virus-infected strains, suggest that AfuPmV-1M induces SG formation, thereby enhancing the fungal host's

readiness to withstand subsequent lethal stress. Alongside SG-related proteins, we have also identified an upregulation of the inner kinetochore protein Mis6 (Afua6g04100) in AfuPmV-1M-infected strain (Af293) under normal physiological conditions, as well as in the virus-cured strain when exposed to oxidative stress (Fig. 4b, d). Mis6, a homolog of human CENP-I, is an essential centromere connector protein, ensuring accurate chromosome alignment, segregation, and proper mitotic progression [28]. Any disruptions in these processes can result in genetic instability and compromises in cell cycle integrity. Numerous viruses manipulate the host cell cycle to establish a favorable environment for replication, often achieved by deregulating key cell cycle checkpoints, including the spindle checkpoint in which Mis6 plays a role [29,30]. Remarkably, human CENP-I is frequently overexpressed and acts as an oncogene in several cancer types [31–33]. This is partly attributed to its cytoprotective properties and role in the DNA damage response [34]. To evaluate the influence of Mis6 upregulation on fungal cell cycle integrity and the DNA damage response, we investigated the ability of virus-infected and virus-cured strains to replicate in the presence of hydroxyurea. Hydroxyurea is a known inhibitor of ribonucleotide diphosphate reductase, which activates the DNA replication checkpoint [35]. Consequently, conidia treated with hydroxyurea should not replicate. Conidia showing signs of initiation of replication, such as the presence of more than one nucleus, are regarded as having defects in mitotic arrest [36].

The virus-infected strains (Af293 and RI) demonstrated increased resistance to hydroxyurea, as indicated by a higher radial growth rate (Fig. 4e). Furthermore, while the virus-infected strains exhibited an intact replication checkpoint, the virus-cured strain (VC) displayed defects in the intra-S-phase checkpoint. This was evident through a higher number of conidia with more than one nucleus and larger, more heterogeneous nucleus size (Fig. f-g, Supplementary Fig. 4). These observations indicate that the AfuPmV-1M-mediated upregulation of Mis6 leads to a more precise control of the cell cycle, and this enhanced regulation may play a role in the increased fitness of the virus-infected strains.

AfuPmV-1M Protects A. fumigatus from Intraphagosomal Killing In vivo Through Intrinsic Cellular Mechanisms

To evaluate the impact of mycoviral infection on fungal fitness in vivo, we conducted a comparative analysis of leukocyte conidial uptake and killing in mice challenged with VI, VC, and RI conidia (Fig. 5a). For this purpose, we employed a mixed infection model in which the three strains were color-coded using an invariant cell wall labeling technique, as previously described [37,38]. This experimental design allowed us to examine the functional

outcomes mediated by intrinsic cell properties in the presence of virus-infected and virus-cured conidia within the same inflammatory milieu. By doing so, we could focus specifically on cell-intrinsic-mediated effects, independent of secondary influences on microbial burden and tissue inflammation that often arise when comparing singly-infected mice. At 24 hours post-infection, the lungs of infected mice were harvested.

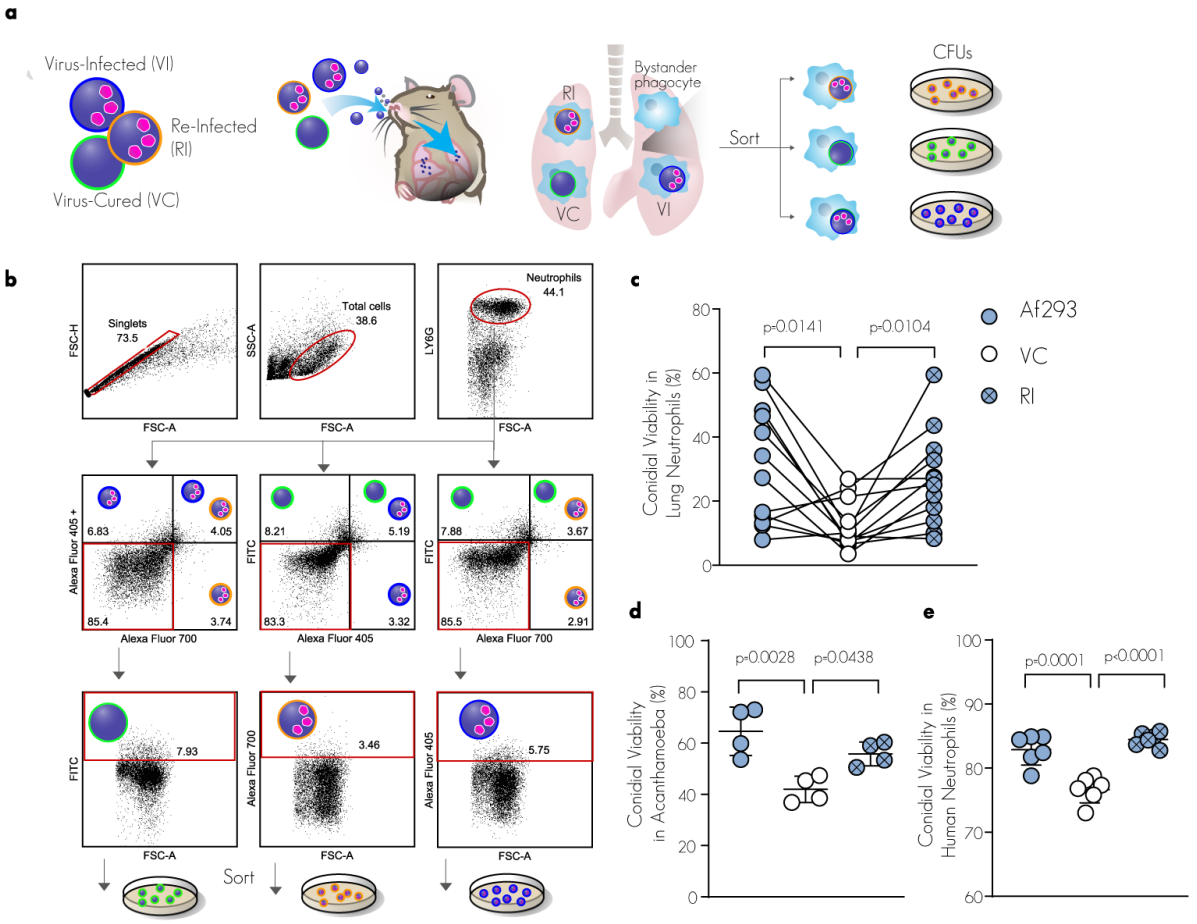

Figure 5. Afupmv-1 regulates conidial survival in phagocytes. a. Mixed infection model. **b.** Gating strategy for sorting neutrophils containing only one conidium of a single strain. Lungs from a naïve animal were used to define the positive populations. **c.** Fungal viability at 24 hours post-infection (p.i.) was calculated based on colony-forming units (CFUs) of sorted neutrophil-phagocytosed strains, including virus-infected, virus-cured (by cycloheximide), and virus re-infected strains. The lines indicate paired data from a single mouse. **d-e.** Swollen conidia were co-incubated with *Acanthamoeba castellanii* **(d)** or human-derived neutrophils **(e)**at MOI of 1:1 for 4 hours. Viability was quantified by CFUs. Statistical analysis: (**c-e**) one-way ANOVA with Tukey's multiple comparison test. Conidial suspensions were adjusted based on viability staining to account for differences in conidial viability prior to each experiment.

Neutrophils containing conidia were identified and sorted into three distinct populations based on their phagocytosis of either virus-infected (VI), virus-cured (VC), or virus re-infected (RI) strains (Fig. 5b, Supplementary Fig. 5a). Phagocytosis by neutrophils was not affected by the presence of the mycovirus, indicating that differences in conidial uptake are unlikely to explain the disparity in fungal virulence (Supplementary Fig. 5b). However, analysis of colony-forming units (CFUs) in the sorted populations revealed enhanced survival of virus-infected conidia (Af293 and RI) within lung neutrophils (Fig. 5c). Similarly, the virus-infected strains (Af293 and RI) demonstrated heightened resistance to conidial killing by human derived neutrophils, and environmental soil-dwelling phagocytes, *Acanthamoeba castellanii*, while phagocytosis remained similar (Fig. 5d-e, Supplementary Fig. 5c). These data provide compelling evidence that AfuPmV-1M bestows protection against neutrophil-mediated conidial killing in the lung. By comparing different strains in the same lung environment, we have established that the cytoprotective effect is cell-intrinsic, ruling out the influence of variations in cell recruitment and inflammatory response.

AfuPmV-1M Promotes Disease Progression

To assess the impact of AfuPmV-1M on virulence, we conducted a challenge experiment using C57BL/6JOlaHsd immunocompetent mice. The mice were inoculated intranasally with 6×10^7 conidia and the results showed a significantly higher mortality rate in the groups infected with virus-infected strains (Af293 and RI) compared to the group infected with the virus-cured strain (Fig. 6a, Supplementary Fig. 6a). The increased mortality observed in the VI and RI groups correlated with elevated fungal burden in the lungs (Fig. 6b) and tissue damage, as indicated by higher levels of lactate dehydrogenase (LDH) in bronchoalveolar lavage fluid (BALF) at 24 hours post-infection (pi) (Fig. 6c). Examination of lung histopathology revealed multiple infection foci and germinating conidia in the virus-infected strain groups (Fig. 6d-e). Following infection with AfuPmV-1M-infected conidia (Af293 and RI), a notable increase was observed in the levels of lung inflammatory cytokines (tumor necrosis factor, IL-1β, IL-6, IFN-β, and IFN-γ) and Myeloperoxidase (MPO) at 72 hours post-infection (hpi) in comparison to infection with the congenic virus-cured conidia (Fig. 6f). These findings suggest a higher degree of tissue inflammation and heightened neutrophil activity, respectively. Taken together, these findings demonstrate that the virus-infected strains exhibit greater virulence than the virus-cured strain, resulting in invasive aspergillosis in immune-competent mice.

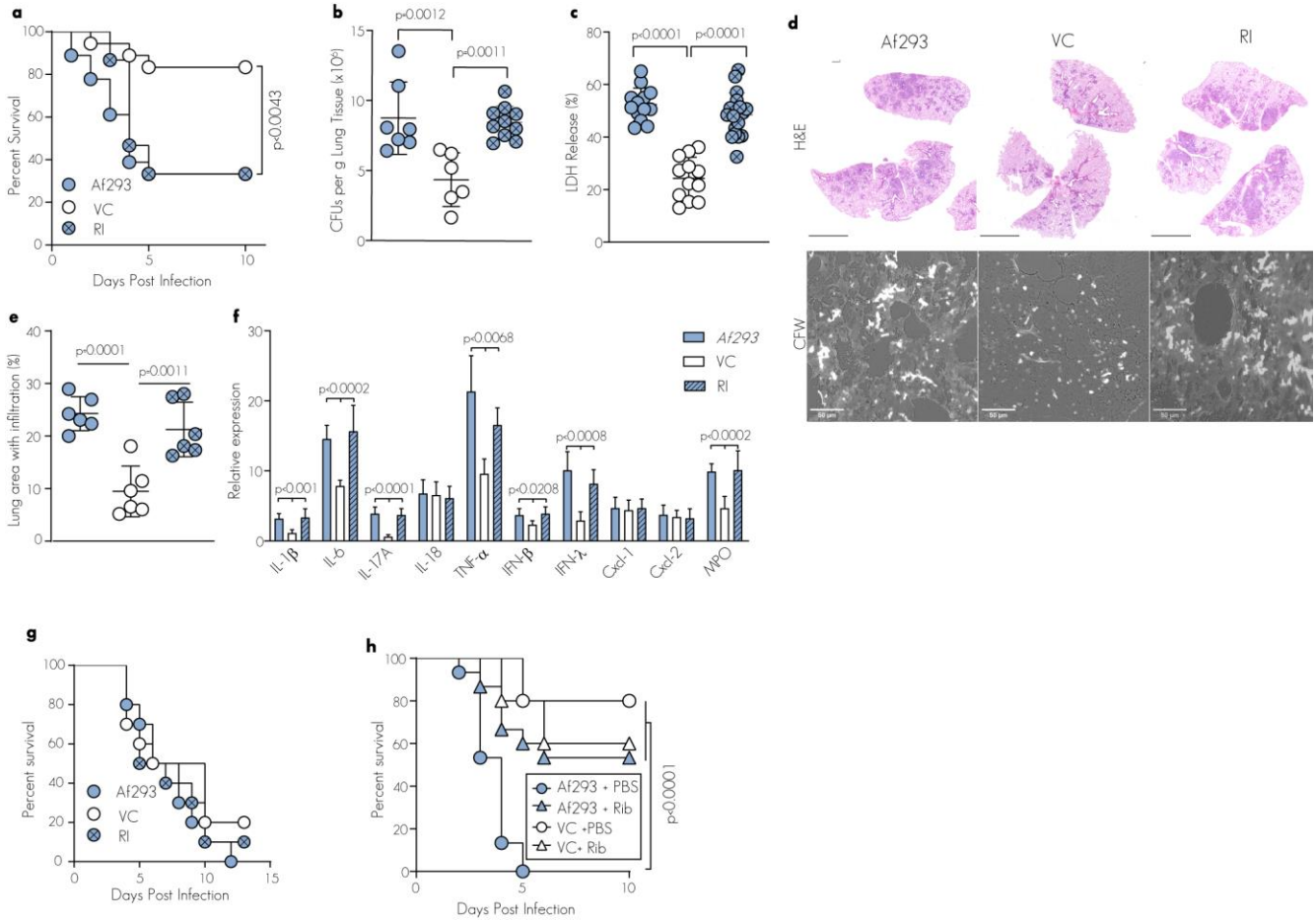

Figure 6. AfuPmV-1 regulates *A. fumigatus* virulence. a. Survival of C57BL/6JOlaHsd mice challenged with 6×10^7 Af293 (n=18), virus-cured by cycloheximide (VC, n=18), or virus re-infected (RI, n=15) conidia. **b.** Lung CFUs at 24h with 3×10^7 conidia. **c.** BALF LDH levels in *A. fumigatus*-challenged mice 48 hours post-inoculation with 6×10^7 conidia. Values are presented as a percentage of LDH release from BALF cells treated with 0.1% Triton X-100 (100% cytotoxicity). **d.** Micrographs of 48 h-infected lung sections stained with hematoxylin and eosin (scale bar, 4 mm) and calcofluor white (scale bar, 50 µm). **e.** Morphometric analysis of lung consolidation (n = 6) at 48 hpi with 6×10^7 conidia. **f.** Relative mRNA expression levels of proinflammatory mediators were assessed via RT-qPCR using total RNA extracted from lung homogenates at 72 hpi in mice infected with the indicated strains (Af293, n=7; VC, n=7; RI, n=6). The data have been normalized to actin expression, and the presented values are relative to the expression levels in naïve lungs. **g.** Survival of p91phox−/− mice challenged with 5×10^4 Af293, VC or RI conidia (n=10 per group). **h.** Survival of mice challenged with 6×10^7 Af293 or VC conidia (pretreated with Ribavirin or PBS for four hours) and treated with 40 mg/kg Ribavirin or vehicle control (PBS) i.p. twice daily. Af293+PBS n=15, Af293+Ribavirin n=15, VC+PBS n=5, VC+ Ribavirin n=5. Statistical analysis: (**a g-h**) Log-rank (Mantel-Cox). (**b-c, e-f**) one-way ANOVA with Tukey's multiple comparison test. Conidial suspensions were adjusted based on viability staining to account for differences in conidial viability prior to each experiment.

AfuPmV-1M cytoprotective effect under oxidative conditions suggests that AfuPmV-1M-mediated resistance to myeloid cell killing is likely related host phagocyte NADPH (reduced form of nicotinamide adenine dinucleotide phosphate) oxidase (i.e., NOX2). Humans with chronic granulomatous disease have genetic defects in NOX2 and a 40% lifetime risk of invasive aspergillosis, highlighting the role of NOX2 in barrier immunity against ubiquitous *A. fumigatus* exposure [39]. To investigate the conjecture that the elevated virulence in the presence of the virus depends on host NADPH oxidase expression, we challenged *p91phox*$^{-/-}$ mice with 5×10^4 Af293, VC, or RI conidia (Fig. 6g). In contrast to *p91phox*$^{+/+}$ mice (Fig. 6a), the survival of *p91phox*$^{-/-}$mice was similar whether Af293, VC, or RI conidia were administered (Fig. 6g). These data show that the virulence of the virus-infected strains is comparable to that of the virus-cured strain in the absence of host NADPH oxidase, confirming that in the absence of oxidative stress the presence of AfuPmV-1M is not advantageous anymore. Thus, AfuPmV-1M confers a survival benefit to the fungal pathogen upon oxidative challenge and within the murine lung.

Antiviral Treatment Reverses the Exacerbated AfuPmV-1M-Mediated Virulence

To assess whether therapeutic intervention to block mycoviral replication could reverse the exacerbated pathology and revert the infectious outcomes, mice were challenged with Af293 or VC conidia and treated intraperitoneally with ribavirin, a nucleoside analog that targets viral replication, twice daily (Fig. 6h). Remarkably, we observed significantly improved survival in Af293-challenged mice treated with ribavirin, suggesting that AfuPmV-1M is a viable target. Therefore, ribavirin and similar antiviral drugs that target viral replication represent promising "antipathogenicity" treatments against virus-bearing pathogenic fungi.

.

Discussion

One key characteristic of mycoviral biology is their absence of a lytic extracellular phase. As a result, mycoviruses are transmitted either vertically, from one generation to the next, or horizontally through hyphal anastomosis [40]. This unique transmission mode creates a dynamic where mycoviruses and their fungal hosts are intricately linked in terms of reproductive success. The presence of anti-mycoviral defense mechanisms in fungi can lead to the elimination of mycoviruses, while enhanced mycoviral virulence may risk driving the fungal host to extinction. Therefore, the delicate equilibrium between mycoviral survival and

the viability of their fungal hosts plays a pivotal role in shaping the dynamics of this complex relationship. In this context, it is reasonable to anticipate the emergence of mutualistic interactions that enhance the reproductive success of both mycoviruses and fungi. Consistent with this notion, the findings of this study exemplify a fungus-mycovirus interaction in which a dsRNA mycovirus provides a survival advantage to the fungus, particularly under environmental stress conditions and within the murine lung.

While mycoviruses have been observed to influence a wide array of phenotypes in plant fungal pathogens [41,42], there is limited knowledge regarding mycoviruses in human pathogenic fungi and their effects on fungal pathogenesis. In this study, we have discovered that the mycovirus AfuPmV-1M in *A. fumigatus* is linked to heightened disease progression and fungal virulence. AfuPmV-1M enhances fungal fitness under oxidative and heat stress conditions, thereby promoting fungal survival within the lung environment, ultimately exacerbating the disease. Our results advance the concept that fungal virulence is multifactorial and is a product of not only fungal and host factors (i.e., NADPH oxidase) but also viral hitchhikers that may act as backseat drivers in determining disease development. Importantly, we introduce a novel therapeutic approach for the first time, focusing on targeting an endogenous virus to diminish the pathogenicity of its host. This is exemplified by our targeting of AfuPmV-1M with the antiviral nucleoside analog Ribavirin (Fig. 6h). Accordingly, antiviral drugs offer great promise as 'antipathogenicity' treatments to mitigate the severity of invasive fungal infections associated with mycoviruses, and to explore the potential of targeting other infections whose pathogenicity might be exacerbated by similar endogenous viruses.

Our data strongly suggest that the hostile phagosomal environment triggers AfupmV-1M replication (Fig. 3f-h). In conjunction with the proteome data (Fig. 4), we propose that the AfuPmV-1M exploits fungal survival pathways through the induction of transcriptional and translational modifications that affect components like stress granules and the DNA damage response, to enhance both fungal survival and its own replication in the face of impending harsh conditions. This, in turn, leads to a modulation of the virulence of the fungal host. Consequently, we propose that chronic AfuPmV-1M infection imposes a mild, non-lethal cellular stress that primes the fungus for subsequent lethal challenges, and thus confers 'cross-tolerance' against different insults such as oxidative stress, which is commonly encountered both in the environment and during infection in a plant or animal host. This proposition is further supported by the observation that among the most highly upregulated proteins under physiological conditions is thioredoxin 1 (Trx1), a pivotal enzyme that shields cells from

oxidative stress by reducing disulfides and methionine sulfoxide groups in oxidized proteins [43].

While the current study is restricted to *A. fumigatus*, our findings may present a general phenomenon in which environmental (biotic and abiotic) and human made stress exert selective pressure for mycoviruses that provide competitiveness by fortifying stress resistance. Accordingly, mycovirus-derived traits that enhance fungal fitness in specialized niches may underlie fungal host adaptation, and account for host-jumps, crossover events, and the emergence of new pathogenic strains from the environment.

Funding

Israeli Science Foundation (ISF) grants 3021/20 and 1760/20

European Research Council (ERC) Starting Grant MycoViralPath 101077734

The Ministry of Science and Technology of Israel 0001998

Author contributions

Conceptualization: VL and NS.

Investigation: VL, MR, JA, HH, and NS.

Funding acquisition: NS.

Supervision: NS.

Writing – original draft: VL and NS.

Writing – review & editing: VL, MR, and NS.

Materials and Methods

Fungal Strains and Growth Conditions

The naturally Afupmv-1M-infected *Aspergillus fumigatus* strain *Af293* was obtained from Dr. Tobias Hohl and kept in our laboratory for over four years. Virus-cured strains (VC) were

generated from *Af293* through treatment with either two cycles of 1mM and 10 mM of the protein synthesis inhibitor cycloheximide or 0.1 mg/ml of the nucleoside analog Ribavirin, as previously described [16,44]. A congenic re-infected strain (RI) was obtained by PEG-mediated transfection of 50 µg of purified AfuPmV-1M dsRNA, extracted from the parental *Af293* strain into the cycloheximide-cured strain (VC) as previously described [44]. All strains were preserved, cultured, and collected for experimentation as previously described [38,45]. For the purification of viral particles and viral dsRNA, fungal cultures were grown in 250 ml of GMM broth with continuous agitation at 130 rpm, at 37°C for a period of 5-7 days. Subsequently, the mycelium was harvested with Miracloth, snap-frozen with liquid nitrogen, and stored at -80°C until subsequent processing.

Purification of Viral particles

The viral particle purification process was conducted as previously described [11] with minor adaptations. Approximately 50 grams 6-day-old mycelia from *A. fumigatus Af293* were homogenized in a 3-fold volume (wt/vol) of 0.1 M sodium phosphate solution at pH 7.4, supplemented with 0.2 M KCl and 0.5% mercaptoethanol using a manual homogenizer (Hangzhou Miu Instruments Co. LTD, type MT-30K). The resulting homogenate was clarified with an equal volume of chloroform followed by centrifugation at 10,000×*g* for 20 minutes at 4°C. The virus-containing supernatant was mixed with 10% (wt/vol) PEG-6000 and 0.6 M NaCl, and incubated overnight at 4°C with constant stirring. The following day, the suspension underwent low-speed centrifugation at 10,000×*g* for 20 minutes. The resulting precipitate, including viral particles, was resuspended in 60 mL of TE buffer and clarified through additional low-speed centrifugation. Any excessive PEG contamination pellet was discarded, while the remaining supernatant, which contained the virus, was subjected to ultracentrifugation at 105,000×*g* for 90 minutes at 4°C. The pellet enriched with virus-like particles (VLPs) was resuspended in 1 mL of TE buffer.

RNA extraction, RT-PCR, and qRT-PCR

Mycelia from liquid shaking cultures were flash-frozen, powdered in liquid nitrogen, and homogenized in Trizol (300 mg mycelia in 1 ml Trizol). For RNA extraction from conidia, conidia were collected from 3 days-old plates and resuspended and homogenized in 1 ml of Trizol. Mycelial and conidial RNA was extracted as previously described [11]. 10 µg of RNA was DNase-treated with TURBO DNA-free (Invitrogen™ # AM1907), according to the

manufacturer's instruction. cDNA was obtained using High-Capacity cDNA Reverse Transcription Kit (Applied Biosystems™ # 4368814). For the expression analysis of viral genes, pretreated with 15% DMSO (v/v) for 10 minutes at 95°C has been used to denature dsRNA prior to the reverse transcription [46]. The presence of targeted genes was confirmed by PCR amplification using Promega GoTaq Green Master Mix. The primers for the individual genes are listed in Supplementary Material (Table S1). qRT-PCR was performed using the Fast SYBR® Green Master Mix (Applied Biosystems™ , # 4385612) and data was collected on an Eppendorf Mastercycler X50a. Gene transcript levels from three biological replicates were quantified by the ΔΔCt method [47], and normalized to *A. fumigatus actA* for measurement of fungal and mycoviral genes and to *actβ* for measurements of murine genes.

Isolation of dsRNA by LiCl precipitation

Total RNA was extracted from *A. fumigatus* 250 ml liquid culture grown at 37°C until saturation, approximately 5 to 6 days. ssRNA/dsRNA fractionation was performed as previously described [48]. To visualize dsRNA, 1 µg were pretreated with RNase-free DNase1 (RBC Bioscience, cat. #9680DN050) and S1 nuclease (Thermo Scientific™, cat. #EN0321) according to the manufacturer's instructions and electrophoresed on 1% agarose gel stained with ethidium bromide.

Whole-genome DNA sequencing and assembly

A. fumigatus genomic DNA was extracted as previously described[49]. Illumina sequencing libraries were prepared by Seqcenter (SeqCenter LLC, PA, USA) using the tagmentation-based and PCR-based Illumina DNA Prep kit and custom IDT 10bp unique dual indices (UDI) with a target insert size of 320 bp. No additional DNA fragmentation or size selection steps were performed. Illumina sequencing was performed on an Illumina NovaSeq 6000 sequencer in one or more multiplexed shared-flow-cell runs, producing 2x151bp paired-end reads. Demultiplexing, quality control and adapter trimming was performed with bcl-convert1 (v4.1.5). The raw FASTQ reads were preprocessed using fastp 0.23.4[50], which entailed removing Illumina adaptor sequences and sequences with low quality scores, specifically those with a Phred score [Q], < 30. Subsequently, the quality of the sequences was assessed using FastQC v0.11.9 (Babraham Institute). Reference-guided genome analysis was conducted on high-quality sequence reads by aligning them to the *A. fumigatus* Af293 reference genome (FungiDB release 66) using Bwa-mem2-2.1[51], followed by conversion to BAM files using samtools 1.16.1[52]. PCR duplicates were identified and marked using the MarkDuplicatesSpark implementation of PicardMarkDuplicates 3.0.0 within GATK v4.4.0.0.

Subsequently, deduplicated BAM files were recalibrated using GATK BaseRecalibrator ApplyBSQ, leveraging known datasets of SNPs derived from the *A. fumigatus* Af293 reference genome. Variant calling for SNP and INDEL identification was carried out using GATKHaplotypecaller v4.4.0.0[53], employing specified parameters, including 'QD < 3.0', 'MQ < 40.0', 'FS > 60.0', 'MQRankSum < -10.0', 'ReadPosRankSum < -5.0' for SNPs, and 'QD < 3.0', 'FS > 200.0', 'ReadPosRankSum < -20.0' for INDELs. Additionally, variants were identified using the Platypus variant caller 0.8.1.2[54], with filter parameters set to a quality filter of 30, a depth filter threshold of 10, and an allele frequency filter threshold of 0.1. Subsequently, variants identified by both variant callers were annotated using SnpEff v4.3[55], followed by intersection, and exclusion of any variants specific to our lab strain AF293. Identified SNPs underwent visual inspection of alignments using IGV version 2.17.0[56] to detect false positive variant calls that may have evaded automated filters.

Stress assays

10^6 conidia/ml conidia of *A. fumigatus Af293*, VC, and RI strains were incubated in GMM broth for 4 hours at 37°C, to obtain swollen conidia. Subsequently, conidia were subjected to stressors including 5mM H_2O_2, pH 4.5, pH 8.5, 50°C, and 1 M Sorbitol for 4 hours at 37°C, 130rpm. Conidial viability was assessed by colony forming units (CFU). To evaluate growth inhibition of *A. fumigatus* strains 10^3 conidia were inoculated onto GMM agar plates under control conditions or at pH 4.5, pH 8.5 and 1M Sorbitol, or 50°C. Diameter of the colony was measured on the 3rd and 7th day of incubation.

Biofilm formation assay

Briefly, 10^6, 10^5, or 10^4 spores in 1% GMM broth were seeded per well in a 24-well microtiter plate with or without voriconazole at the indicated concentration were incubated at 37°C for 48 hours. To determine the biofilm formation ability of *A. fumigatus* strains, we conducted the crystal violet (CV) assay as previously described [57] with minor modifications. 1 mL of GMM broth with and without the voriconazole was inoculated with 10^6, 10^5, and 10^4 conidia in a 24-well microtiter plate, and incubated at 37°C for 48 hours. The plate was then washed twice with PBS to eliminate free-floating cells, and the biofilms were stained with 1 mL of 0.1% crystal violet solution for 10 minutes at room temperature. Biomass was washed with PBS at least 5 times and air-dried, followed by incubation with 1 mL of 100% acetic acid, slightly shaken at room temperature for 30 minutes to elute the crystal violet, and the absorbance was measured at 470 nm using a Tecan Infinite Pro Plate reader.

Phagocytosis assay

Human neutrophils were harvested and *Acanthamoeba castellanii* were maintained as previously described [58,59]. For the phagocytosis and survival assay with either amoeba or human neutrophils, 1×10^6 phagocytes were plated in a 24-well plate containing 1 ml of supplemented DMEM (human neutrophils) or PYG (amoeba) medium and pre-incubated for 1 hour letting amoebal cells attach to the surface. The cell walls of swollen conidia (4 hours in GMM at 37°C) were fluorescently labeled with Alexafluor 488-conjugated streptavidin as previously described (reference). 1×10^6 labeled *A. fumigatus* conidia were inoculated into the neutrophil and amoeba culture and incubated for 4 hours at 37°C under 5% CO2 (neutrophils) or 30°C (*A. castellanii)*. Phagocytosis was evaluated by flow cytometry. The phagocytes' population was gated by size, and the AF488 $^+$ population represents conidial uptake. Conidial viability was evaluated by colony forming units (CFUs).

Conidiation and Germination assays

Conidiation was quantified by harvesting conidia from 4 days old GMM agar plates that were inoculated with 2×10^5 conidia. The conidial concentration was determined by counting with a hemocytometer. To determine the germination rate, conidia were collected from 5 days-old GMM plates, adjusted to 5×10^5 conidia per ml in GMM broth and inoculated in 8 wells microscopy chambered slide at 37°C. Images were captured using an inverted motorized Nikon fluorescence microscope (Eclipse Ti2) in time-lapse mode, with 30 minutes frame over a period of 24 hours.

Inspection of fungal lawn and visualization of conidiophores

For evaluation of fungal lawn morphology, 200 ul of 10^6 conidia/ml was spread onto GMM agar plates and incubated for 7 days at 37°C. 10 ul of 2×10^6 conidia were inoculated into agar slices and covered by a sterile coverslip. After 2 and 3 days after inoculation, glasses with attached conidiophores were gently detached from the agar slice, placed on microscopy glass with lactophenol blue, and sealed by polish. Conidiophores were visualized by ×100 microscopy (Nikon, Eclipse Ti2), photos were captured and conidia on individual conidiophores were counted.

Mice, Animal Care, and Ethics Statement

6-8 weeks-old C57BL/6JOlaHsd mice were purchased from Envigo, Israel. p91phox-/- mice were originally obtained from The Jackson Laboratory (strain 002365) and bred under specific pathogen-free conditions at our mouse facility at the Hebrew University of Jerusalem. All animal experiments were conducted with sex- and age-matched mice and are compatible with the standards for care and use of laboratory animals. The research has been approved by the Hebrew University of Jerusalem Institutional Animal Care and Use Committee (IACUC) (protocol number MD-20-16072-5). The Hebrew University of Jerusalem is accredited by the NIH and by AAALAC to perform experiments on laboratory animals (NIH approval number: OPRR-A01-5011).

Analysis of Infected Mice

Mice were infected via the intranasal route as described in [45]. In assays where labeled conidia were used, the conidia were labeled as previously described [37]. BAL and lung suspensions were prepared for flow cytometry as described in [38]. Briefly, lung digest and, if applicable, BAL cells were enumerated and stained with the following Abs: anti-Ly6C (clone AL-21), anti-Ly6G (clone 1A8), anti-CD11b (clone M1/70), anti-CD11c (clone HL3), anti-CD45.2 (clone 104), anti-MHC class II (clone M5/114.15.2), anti-Siglec F (clone E50-2440) and anti-CD103 (clone 2E7). Neutrophils were identified as $CD45^{+}CD11b^{+}Ly6C^{lo}Ly6G^{+}$ cells, inflammatory monocytes as $CD45^{+}CD11b^{+}Ly6C^{hi}Ly6G^{-}$ cells, Mo-DCs as $CD45^{+}CD11c^{+}$MHC class II^{+} $CD11b^{+}CD103^{-}SiglecF^{-}$ cells, and alveolar macrophages as $SSC^{hi}CD45^{+}CD11b^{+}CD11c^{+}$ $SiglecF^{+}$ bronchoalveolar lavage (BAL) fluid cells. Flow cytometry data was collected on a NovoCyte Quanteon (Agilent Technologies Inc) flow cytometer and analyzed on NovoExpress v1.5.0 (Agilent Technologies Inc). Neutrophils containing ingested labeled conidia were sorted using the BD FACSAria™ III (BD Biosciences, San Jose, CA). BAL Lactate dehydrogenase (LDH) levels were measured with a CytoTox 96 Non-Radioactive Cytotoxicity Assay (Promega, Madison, WI).
Perfused murine lungs were homogenized in 2 mL of PBS, 0.025% Tween-20 for colony-forming units (CFUs) and ELISA. For histology, perfused lungs were fixed in 10% neutral-buffered formalin, embedded in paraffin, sectioned in 4 μm slices, and stained with hematoxylin & eosin (H&E) or calcofluor white (MP Biomedicals). Slides were reviewed and evaluated in a blinded manner. Whole section images were digitally scanned using a Nanozoomer S360 slides scanner.

Liquid chromatography–MS/MS

Liquid chromatography–MS/MS was performed at The De Botton Protein Profiling institute of the Nancy and Stephen Grand Israel National Center for Personalized Medicine, Weizmann Institute of Science. 10^6 conidia per ml were cultured in 75 ml of GMM broth for 18 hours, followed by a 4-hour oxidative stress challenge with 8 mM of H_2O_2. The resulting mycelium was ground in liquid nitrogen and then resuspended in a 5% SDS buffer. The samples underwent in-solution tryptic digestion using the S-trap protocol developed by Protifi. The resulting peptides were subjected to analysis using nanoflow liquid chromatography (nanoElute) coupled to a high-resolution, high-mass-accuracy mass spectrometry system (Bruker Tims TOF Pro). During analysis, the samples were randomly ordered in discovery mode. The raw data was processed with FragPipe v17.1. The data was searched with the MSFragger search engine against the NCBI *Aspergillus fumigatus* Af293 proteome, appended with common lab protein contaminants. Carbamidomethyl was specified as a fixed modification. Oxidation of methionine residues and protein N-terminal acetylation were specified as a variable modification. The quantitative comparisons were calculated using Perseus v1.6.0.7. Decoy hits were filtered out and only proteins detected in at least 2 replicates of at least one experimental group were kept.

Mitosis Assay

To evaluate the genetic stability of *A. fumigatus* strains, we conducted mitosis assay as previously described [36]. Briefly, A total of $1x10^5$ conidia from Af293, VC, and RI strains were inoculated in a 30 mm petri dish containing 3 ml of liquid YG supplemented with 100 mM hydroxyurea (HU) and incubated at 37°C. After a 5-hour incubation the germlings were released from cell-cycle arrest by four washes with YG medium, and then incubated in fresh YG (without HU) at 37°C for the indicated periods. For nuclei visualization, cells were treated for 5 min with 20 µg/ml of Hoechst 33342 (Invitrogen). After staining, coverslips were washed twice with PBS and analyzed on an inverted motorized Nikon fluorescence microscope (Eclipse Ti2) using a 100× objective oil immersion lens.

Statistics and Reproducibility

All statistical analysis was performed in GraphPad Prism 8. Unless otherwise noted, all statistical analyses were performed with a minimum of three biologically independent

samples. All images are representative of a minimum of three biologically independent samples that represent a minimum of three independent experimentations unless otherwise noted. For comparisons between two groups two-tailed unpaired t-tests were performed. For comparisons between greater than two groups One-Way ANOVA with Tukey, Sidak, or Dunnett post tests for multiple comparisons were performed. All error bars indicate standard error and are centered around the mean.

Supplementary Figures

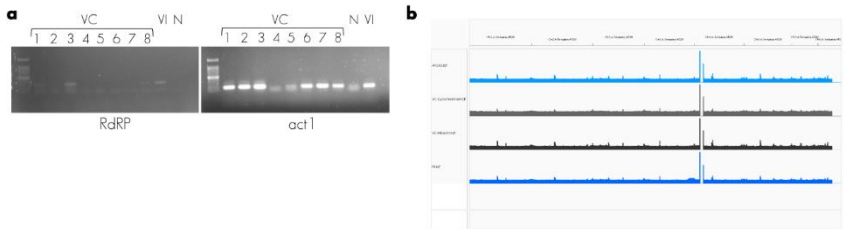

Figure S1. Generation of congenic Ribavirin virus-cured strains and whole genome sequencing. a. Reverse-transcription PCR (RT-PCR) amplification of a 276 bp segment from Afupmv-1M RdRP in total RNA extracted from Af293 (VI) and Ribavirin virus-cured (VC). N-negative control. **b**. Genomic comparisons of *A. fumigatus* virus-infected, virus-cured and re-infected strains compared to the reference strain Af293.

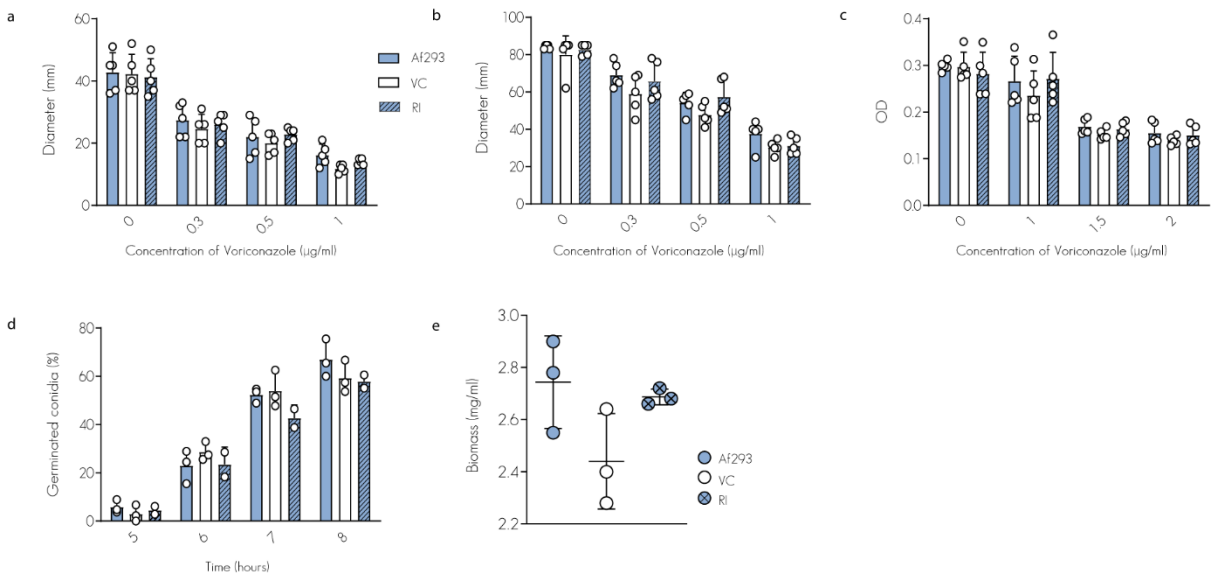

Figure S2. Characterization of the Afupmv-1M-cured and re-infected strains. Radial growth of Af293, cycloheximide-cured, and the re-infected strains on GMM plates amended with Voriconazole

three days (a) and seven days (b) post-inoculation. **c**. Biofilm formation on a plastic surface in the presence of Voriconazole after 48 hours of incubation at 37°C. **d**. Germination rate of conidia. **e**. Fungal biomass production over 24 hours of incubation. Conidial suspensions were adjusted based on viability staining to account for differences in conidial viability before each experiment.

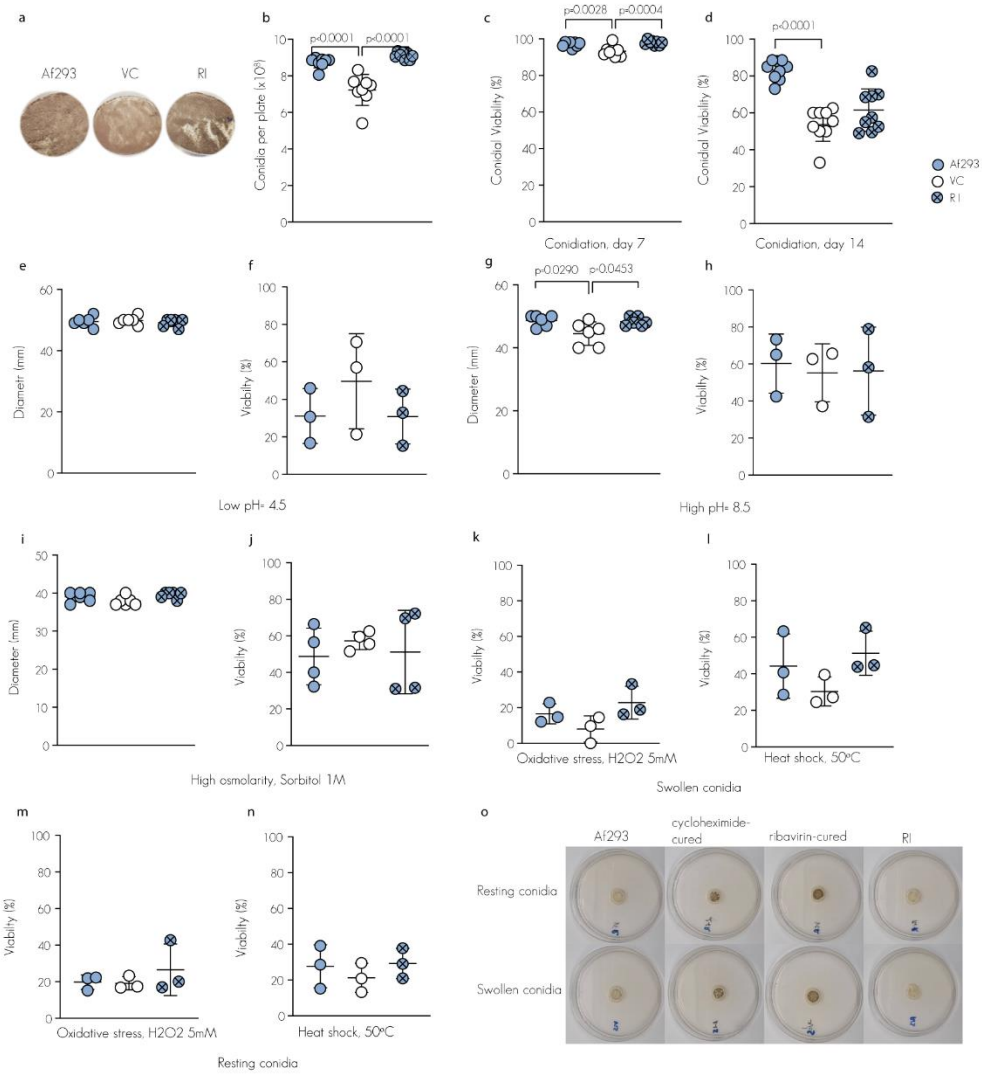

Figure S3. Conidiation and conidial viability. a. The AfuPmV-1M-infected strain (Af293) exhibits darker colonies compared to the Ribavirin virus-cured strain. 2×10^5 conidia (CFUs) were spread over GMM plates and grown for 7 days. **b**. Quantification of conidia number per plate. 2×10 **c**. Conidial viability during conidiation. 2×10^5 *Af293* and Ribavirin virus-cured (VC) conidia (CFUs) were spread on GMM plates and grown for 5 days. Conidia were then harvested, stained with propidium iodide, and analyzed by flow cytometry. **d**. Conidial viability of Virus-infected and cycloheximide-cured strains during conidiation on 14th day. **e-f**. Growth rate of 10^4 conidia (e) and viability of swollen for 4 hours conidia (f) on GMM media with low pH= 4.5**. g-h**. Growth rate of 10^4 conidia (g) and viability of swollen for 4 hours conidia (h) on GMM media with high pH= 8.5**. i-j**. Growth rate of 10^4 conidia (i) viability of swollen for 4 hours conidia (j) on GMM media with osmotic stress 1 M Sorbitol. **K-l.** Swollen virus-infected (Af293 and RI) or ribavirin virus-cured conidia (4 h) were exposed to 5 mM H_2O_2 (k) or 50°C (l) for an additional 4 h and analyzed for CFUs. **m-n**. Resting virus-infected (Af293 and RI) or ribavirin virus-cured conidia were exposed to 5 mM H_2O_2 (m) or 50°C (n) for 4 hours and analyzed for CFUs.

o. 2×10^5 conidia (CFUs) were spread over GMM plates and grown for 3 days at 50°C. The virus-cured (VC) strains exhibit increased conidiation under heat stress compared to the Afupmv-1M-infected strains. Conidial suspensions were adjusted based on viability staining to account for differences in conidial viability prior to each experiment.

Dataset 1. Total spectra of *A. fumigatus* virus-infected and virus-cured strains using *Aspergillus fumigatus Af293* database.

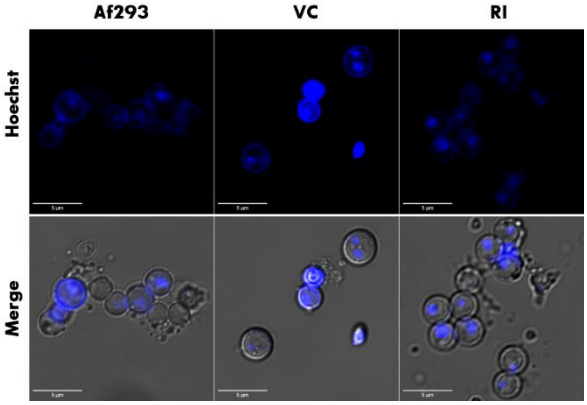

Figure S4. Mitosis Assay. Conidia were grown for 5 hours at 37°C in complete medium (YG) + 100 mM hydroxyurea, then washed and incubated in YG medium for 120 minutes. Conidia were stained with Hoechst and analyzed by microscopy (scale bar, 5 µm).

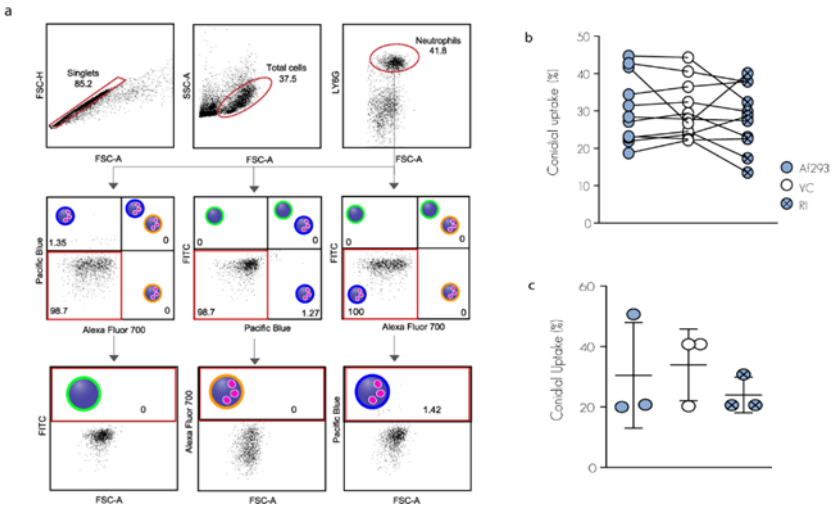

Figure S5. The gating strategy for isolating neutrophils involved utilizing lung samples from an unexposed animal to establish the criteria for identifying the positive cell populations. (a) Uptake of Virus- infected and Virus -cured conidia by sorted murine neutrophil. The lines indicate paired data from a single mouse. (b) Uptake of swollen conidia by environmental phagocytes *Acanthamoeba castellanii* (c).

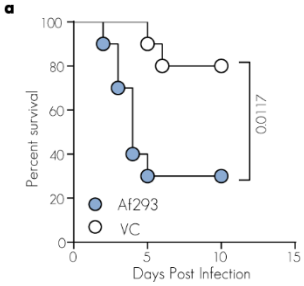

Figure S6. AfuPmV-1 regulates *A. fumigatus* virulence. a. Survival of C57BL/6JOlaHsd mice challenged with 6×10^7 *Af293* (n=10) or virus-cured by ribavirin (VC, n=10) conidia.

References:

1. Fisher, M. C., Hawkins, N. J., Sanglard, D. & Gurr, S. J. Worldwide emergence of resistance to antifungal drugs challenges human health and food security. *Science* **360**, 739–742 (2018).
2. Bongomin, F., Gago, S., Oladele, R. O. & Denning, D. W. Global and Multi-National Prevalence of Fungal Diseases-Estimate Precision. *J Fungi Basel* **3**, (2017).
3. Paulussen, C. *et al.* Ecology of aspergillosis: insights into the pathogenic potency of Aspergillus fumigatus and some other Aspergillus species. *Microb Biotechnol* **10**, 296–322 (2017).
4. Myers, J. M. *et al.* Survey of Early-Diverging Lineages of Fungi Reveals Abundant and Diverse Mycoviruses. *mBio* **11**, e02027-20 (2020).
5. Wu, M. *et al.* Characterization of a novel bipartite double-stranded RNA mycovirus conferring hypovirulence in the phytopathogenic fungus Botrytis porri. *J. Virol.* **86**, 6605–6619 (2012).
6. Lau, S. K. *et al.* Novel partitivirus enhances virulence of and causes aberrant gene expression in Talaromyces marneffei. *MBio* **9**, e00947-18 (2018).
7. Sass, G., Kotta-Loizou, I., Martinez, M., Larwood, D. J. & Stevens, D. A. Polymycovirus Infection Sensitizes Aspergillus fumigatus for Antifungal Effects of Nikkomycin Z. *Viruses* **15**, 197 (2023).
8. Nerva, L. *et al.* Mycoviruses mediate mycotoxin regulation in Aspergillus ochraceus. *Environ. Microbiol.* **21**, 1957–1968 (2019).

9. Ninomiya, A. *et al.* Mycovirus-Induced Tenuazonic Acid Production in a Rice Blast Fungus Magnaporthe oryzae. *Front. Microbiol.* **11**, 1641 (2020).
10. Márquez, L. M., Redman, R. S., Rodriguez, R. J. & Roossinck, M. J. A virus in a fungus in a plant: three-way symbiosis required for thermal tolerance. *Science* **315**, 513–5 (2007).
11. Kanhayuwa, L., Kotta-Loizou, I., Özkan, S., Gunning, A. P. & Coutts, R. H. A. A novel mycovirus from Aspergillus fumigatus contains four unique dsRNAs as its genome and is infectious as dsRNA. *Proc. Natl. Acad. Sci.* **112**, 9100–9105 (2015).
12. Takahashi-Nakaguchi, A. *et al.* Phenotypic and molecular biological analysis of polymycovirus AfuPmV-1M from Aspergillus fumigatus: Reduced fungal virulence in a mouse infection model. *Front. Microbiol.* **11**, 3223 (2020).
13. Clancey, S. A. *et al.* A Novel Mycovirus Evokes Transcriptional Rewiring in the Fungus Malassezia and Stimulates Beta Interferon Production in Macrophages. *mBio* **11**, e01534-20 (2020).
14. Park, M. *et al.* A novel virus alters gene expression and vacuolar morphology in Malassezia cells and induces a TLR3-mediated inflammatory immune response. *Mbio* **11**, e01521-20 (2020).
15. Cao, C., Li, H., Jones, M. G. K. & Wylie, S. J. Challenges to elucidating how endornaviruses influence fungal hosts: Creating mycovirus-free isogenic fungal lines and testing them. *J. Virol. Methods* **274**, 113745 (2019).
16. Ikeda, A., Chiba, Y., Kuroki, M., Urayama, S. & Hagiwara, D. Efficient elimination of RNA mycoviruses in aspergillus species using RdRp-inhibitors ribavirin and 2'-C-methylribonucleoside derivatives. *Front. Microbiol.* **13**, 1024933 (2022).
17. Gouge, J. *et al.* Molecular mechanisms of Bdp1 in TFIIIB assembly and RNA polymerase III transcription initiation. *Nat. Commun.* **8**, 130 (2017).
18. Kedersha, N. *et al.* Stress granules and processing bodies are dynamically linked sites of mRNP remodeling. *J. Cell Biol.* **169**, 871–884 (2005).
19. Reineke, L. C. & Lloyd, R. E. Diversion of stress granules and P-bodies during viral infection. *Virology* **436**, 255–267 (2013).

20. Onomoto, K. *et al.* Critical Role of an Antiviral Stress Granule Containing RIG-I and PKR in Viral Detection and Innate Immunity. *PLoS ONE* **7**, e43031 (2012).

21. Jain, S. *et al.* ATPase-Modulated Stress Granules Contain a Diverse Proteome and Substructure. *Cell* **164**, 487–498 (2016).

22. Schaefer, M. *et al.* RNA methylation by Dnmt2 protects transfer RNAs against stress-induced cleavage. *Genes Dev.* **24**, 1590–1595 (2010).

23. Kimball, S. R., Horetsky, R. L., Ron, D., Jefferson, L. S. & Harding, H. P. Mammalian stress granules represent sites of accumulation of stalled translation initiation complexes. *Am. J. Physiol.-Cell Physiol.* **284**, C273–C284 (2003).

24. Markmiller, S. *et al.* Context-Dependent and Disease-Specific Diversity in Protein Interactions within Stress Granules. *Cell* **172**, 590-604.e13 (2018).

25. Kedersha, N. *et al.* Evidence That Ternary Complex (eIF2-GTP-tRNA $_i^{Met}$)–Deficient Preinitiation Complexes Are Core Constituents of Mammalian Stress Granules. *Mol. Biol. Cell* **13**, 195–210 (2002).

26. Reineke, L. C., Kedersha, N., Langereis, M. A., Van Kuppeveld, F. J. M. & Lloyd, R. E. Stress Granules Regulate Double-Stranded RNA-Dependent Protein Kinase Activation through a Complex Containing G3BP1 and Caprin1. *mBio* **6**, e02486-14 (2015).

27. Protter, D. S. W. & Parker, R. Principles and Properties of Stress Granules. *Trends Cell Biol.* **26**, 668–679 (2016).

28. Takahashi, K., Chen, E. S. & Yanagida, M. Requirement of Mis6 Centromere Connector for Localizing a CENP-A-Like Protein in Fission Yeast. *Science* **288**, 2215–2219 (2000).

29. Bagga, S. & Bouchard, M. J. Cell Cycle Regulation During Viral Infection. in *Cell Cycle Control* (eds. Noguchi, E. & Gadaleta, M. C.) vol. 1170 165–227 (Springer New York, New York, NY, 2014).

30. Fan, Y., Sanyal, S. & Bruzzone, R. Breaking Bad: How Viruses Subvert the Cell Cycle. *Front. Cell. Infect. Microbiol.* **8**, 396 (2018).

31. Ding, N., Li, R., Shi, W. & He, C. CENPI is overexpressed in colorectal cancer and regulates cell migration and invasion. *Gene* **674**, 80–86 (2018).

32. Wang, J. *et al.* Centromere Protein I (CENP-I) Is Upregulated in Gastric Cancer, Predicts Poor Prognosis, and Promotes Tumor Cell Proliferation and Migration. *Technol. Cancer Res. Treat.* **20**, 153303382110455 (2021).

33. Thangavelu, P. U. *et al.* Overexpression of the E2F target gene *CENPI* promotes chromosome instability and predicts poor prognosis in estrogen receptor-positive breast cancer. *Oncotarget* **8**, 62167–62182 (2017).

34. Dang, T. T. & Morales, J. C. Loss of CENP-I Impairs Homologous Recombination and Sensitizes Cells to PARP1 Inhibition. *Cancers* **13**, 3202 (2021).

35. Alvino, G. M. *et al.* Replication in Hydroxyurea: It's a Matter of Time. *Mol. Cell. Biol.* **27**, 6396–6406 (2007).

36. Dos Reis, T. F. *et al.* The Influence of Genetic Stability on *Aspergillus fumigatus* Virulence and Azole Resistance. *G3 GenesGenomesGenetics* **8**, 265–278 (2018).

37. Jhingran, A. *et al.* Tracing conidial fate and measuring host cell antifungal activity using a reporter of microbial viability in the lung. *Cell Rep* **2**, 1762–73 (2012).

38. Shlezinger, N. *et al.* Sterilizing immunity in the lung relies on targeting fungal apoptosis-like programmed cell death. *Science* **357**, 1037–1041 (2017).

39. Holland, S. M. Chronic Granulomatous Disease. *Clin. Rev. Allergy Immunol.* **38**, 3–10 (2010).

40. Kotta-Loizou, I. & Coutts, R. H. A. Mycoviruses in Aspergilli: A Comprehensive Review. *Front. Microbiol.* **8**, (2017).

41. Kotta-Loizou, I. Mycoviruses and their role in fungal pathogenesis. *Curr. Opin. Microbiol.* **63**, 10–18 (2021).

42. Ali, A. Fungal viruses: an unlikely ally. in *Applied Plant Virology* 229–236 (Elsevier, 2020). doi:10.1016/B978-0-12-818654-1.00017-7.

43. Meyer, Y., Buchanan, B. B., Vignols, F. & Reichheld, J.-P. Thioredoxins and Glutaredoxins: Unifying Elements in Redox Biology. *Annu. Rev. Genet.* **43**, 335–367 (2009).

44. Bhatti, M. F. *et al.* The effects of dsRNA mycoviruses on growth and murine virulence of Aspergillus fumigatus. *Fungal Genet. Biol.* **48**, 1071–1075 (2011).

45. Shlezinger, N. & Hohl, T. M. Mitochondrial Reactive Oxygen Species Enhance Alveolar Macrophage Activity against Aspergillus fumigatus but Are Dispensable for Host Protection. *Msphere* **6**, e00260-21 (2021).

46. Crabtree, A. *et al.* A Rapid Method for Sequencing Double-Stranded RNAs Purified from Yeasts and the Identification of a Potent K1 Killer Toxin Isolated from Saccharomyces cerevisiae. *Viruses* **11**, 70 (2019).

47. Livak, K. J. & Schmittgen, T. D. Analysis of Relative Gene Expression Data Using Real-Time Quantitative PCR and the 2−ΔΔCT Method. *Methods* **25**, 402–408 (2001).

48. Levanova, A. & Poranen, M. M. Application of steric exclusion chromatography on monoliths for separation and purification of RNA molecules. *J. Chromatogr. A* **1574**, 50–59 (2018).

49. Biel, S. W. & Parrish, F. W. Isolation of DNA from fungal mycelia and sclerotia without use of density gradient ultracentrifugation. *Anal. Biochem.* **154**, 21–25 (1986).

50. Chen, S., Zhou, Y., Chen, Y. & Gu, J. fastp: an ultra-fast all-in-one FASTQ preprocessor. *Bioinformatics* **34**, i884–i890 (2018).

51. Vasimuddin, Md., Misra, S., Li, H. & Aluru, S. Efficient Architecture-Aware Acceleration of BWA-MEM for Multicore Systems. in *2019 IEEE International Parallel and Distributed Processing Symposium (IPDPS)* 314–324 (IEEE, Rio de Janeiro, Brazil, 2019). doi:10.1109/IPDPS.2019.00041.

52. Danecek, P. *et al.* Twelve years of SAMtools and BCFtools. *GigaScience* **10**, giab008 (2021).

53. McKenna, A. *et al.* The Genome Analysis Toolkit: A MapReduce framework for analyzing next-generation DNA sequencing data. *Genome Res.* **20**, 1297–1303 (2010).

54. WGS500 Consortium *et al.* Integrating mapping-, assembly- and haplotype-based approaches for calling variants in clinical sequencing applications. *Nat. Genet.* **46**, 912–918 (2014).

55. Cingolani, P. *et al.* A program for annotating and predicting the effects of single nucleotide polymorphisms, SnpEff: SNPs in the genome of Drosophila melanogaster strain w ^{1118} ; iso-2; iso-3. *Fly (Austin)* **6**, 80–92 (2012).

56. Thorvaldsdottir, H., Robinson, J. T. & Mesirov, J. P. Integrative Genomics Viewer (IGV): high-performance genomics data visualization and exploration. *Brief. Bioinform.* **14**, 178–192 (2013).

57. Liu, L. *et al.* Calcineurin signaling pathway influences Aspergillus niger biofilm formation by affecting hydrophobicity and cell wall integrity. *Biotechnol. Biofuels* **13**, 54 (2020).

58. Antonio, M.-B., Alma Y, A.-M., Edgar I, M.-Z., Rubi C, C.-M. & Maricruz J, M.-R. Simplified Neutrophil Isolation Protocol. *Int. J. Immunol. Immunother.* **7**, (2020).

59. Segal, G. & Shuman, H. A. Legionella pneumophila Utilizes the Same Genes To Multiply within Acanthamoeba castellanii and Human Macrophages. *Infect. Immun.* **67**, 2117–2124 (1999).

Protein	Organism	Description	Combined Total Peptides	p-value VC_H2O2/ VC	q-value VC_H2O2/ VC	Ratio VC_H2O2/ VC	p-value Af293_H2O2/ Af293	q-value Af293_H2O2/ Af293	Ratio Af293_H2O2/ Af293	p-value Af293/VC	q-value Af293/VC	Ratio Af293/VC	p-value VC_H2O2/ Af293_H2O2	q-value VC_H2O2/ Af293_H2O2	Ratio VC_H2O2/ Af293_H2O2	Intensity: VC 1	Intensity: VC 2	Intensity: VC 3	Intensity: VC_1 H2O2	Intensity: VC_2 H2o2	Intensity: VC_3 H2O2	Intensity: Af293 1	Intensity: Af293 2	Intensity: Af293 3	Intensity: Af293_1 H2o2	Intensity: Af293_2 H2O2	Intensity: Af293_3 H2O2	Combined Spectral Count	Combined Unique Spectral Count	Combined Total Spectral Count	Protein Probability
XP 754348.1	Aspergillus fumigatus Af293	transcription factor TFIIIB complex subunit Brf1	6	0.001979	0.038989	**12.7**	0.609383	0.749169	**0.7**	0.002332	0.362240	**11.0**	0.502195	0.903358	**1.8**	1.47E+04	2.41E+04	7.77E+03	2.07E+05	1.37E+05	1.98E+05	1.23E+05	1.63E+05	1.82E+05	2.24E+05	2.08E+05	2.16E+04	35	35	35	1
XP 746888.1	Aspergillus fumigatus Af293	C6 transcription factor, putative	2	0.181677	0.255788	**4.6**	0.063630	0.144347	**0.1**	0.030305	0.351235	**0.4**	0.256634	0.780998	**3.9**	8.19E+04	1.39E+04	1.05E+04	2.18E+05	2.63E+04	2.03E+05	1.94E+05	2.10E+05	1.71E+05	1.11E+04	1.24E+05	1.39E+04	7	7	7	0.9714
XP 746633.1	Aspergillus fumigatus Af293	conserved hypothetical protein	4	0.539546	0.674592	**0.5**	0.000025	0.200000	**0.1**	0.147461	0.482979	**5.1**	0.483170	0.896297	**0.9**	1.68E+04	1.52E+04	2.45E+05	1.93E+04	2.59E+04	1.98E+04	1.87E+05	2.27E+05	1.99E+05	2.34E+04	2.71E+04	2.07E+04	10	10	10	1
XP 751602.1	Aspergillus fumigatus Af293	ESCRT-I complex component Vps25l, putative	3	0.025954	0.062481	**3.5**	0.113036	0.237055	**0.4**	0.001240	0.360286	**5.1**	0.440278	0.878882	**1.6**	7.98E+03	1.30E+04	8.72E+03	1.76E+04	4.51E+04	5.02E+04	6.34E+04	4.33E+04	4.25E+04	2.28E+04	1.04E+04	4.31E+04	14	14	14	1
XP 747667.2	Aspergillus fumigatus Af293	Mid1 domain protein	5	0.001894	0.038994	**8.1**	0.041226	0.122345	**0.2**	0.045255	0.365304	**4.3**	0.001083	0.464133	**7.9**	1.34E+04	1.53E+04	2.86E+04	1.05E+05	1.62E+05	1.82E+05	5.06E+04	4.77E+04	1.87E+05	1.36E+04	1.80E+04	2.54E+04	19	19	19	1
XP 754127.1	Aspergillus fumigatus Af293	thioredoxin Trx1, putative	3	0.155720	0.697110	**1.2**	0.009409	0.064535	**0.4**	0.003802	0.294723	**4.0**	0.294670	0.792550	**0.8**	1.10E+04	1.87E+04	2.26E+04	1.77E+04	2.34E+04	1.75E+04	5.68E+04	7.10E+04	7.26E+04	2.04E+04	2.10E+04	3.68E+04	16	16	16	0.9985
XP 753581.1	Aspergillus fumigatus Af293	voltage-gated chloride channel, putative	4	0.056336	0.103003	**4.1**	0.105987	0.196971	**0.2**	0.058750	0.380976	**4.0**	0.102415	0.712598	**5.5**	1.44E+05	2.72E+04	3.36E+04	2.24E+05	1.79E+05	2.20E+05	1.85E+05	2.18E+05	2.02E+05	1.87E+05	1.50E+04	1.86E+04	12	12	12	0.9965
XP 747804.1	Aspergillus fumigatus Af293	MFS transporter, putative	4	0.008529	0.038571	**4.1**	0.628998	0.764725	**0.9**	0.013759	0.330676	**3.1**	0.231559	0.768025	**1.5**	1.11E+04	1.58E+04	2.69E+04	6.85E+04	5.91E+04	7.98E+04	5.46E+04	6.11E+04	4.42E+04	6.26E+04	5.74E+04	2.58E+04	29	29	29	1
XP 753760.1	Aspergillus fumigatus Af293	conserved hypothetical protein- Ribosomal prot	3	0.023753	0.061265	**2.8**	0.126963	0.229711	**0.4**	0.020437	0.352803	**3.1**	0.128889	0.713962	**2.1**	1.93E+04	1.34E+04	3.57E+04	5.40E+04	5.74E+04	6.82E+04	7.31E+04	8.17E+04	4.45E+04	3.22E+04	5.13E+04	1.40E+04	23	23	23	1
XP 751486.1	Aspergillus fumigatus Af293	RNA methyltransferase, Trm9 family family	5	0.032774	0.071614	**2.5**	0.219067	0.343384	**0.5**	0.011361	0.317290	**3.0**	0.354025	0.832628	**1.7**	1.77E+04	1.20E+04	9.28E+03	2.04E+04	4.02E+04	3.82E+04	4.18E+04	2.73E+04	4.55E+04	9.87E+03	4.39E+04	1.54E+04	11	11	11	1
XP 748920.1	Aspergillus fumigatus Af293	MOSC domain protein	3	0.278190	0.370032	**0.4**	0.003314	0.057734	**0.2**	0.238115	0.566649	**2.6**	0.632551	0.937077	**0.9**	1.15E+04	1.03E+05	7.30E+04	2.43E+04	1.56E+04	1.68E+04	1.29E+05	1.08E+05	1.07E+05	1.30E+04	2.46E+04	3.10E+04	8	8	8	1
XP 001481470.1	Aspergillus fumigatus Af293	sodium bile acid symporter family protein	3	0.891467	0.942158	**1.1**	0.596306	0.739442	**0.8**	0.011424	0.318190	**2.6**	0.385234	0.852312	**0.5**	2.10E+04	1.59E+04	1.91E+04	1.15E+04	1.12E+04	6.39E+04	4.65E+04	3.43E+04	6.76E+04	4.66E+04	5.89E+04	2.06E+04	13	13	13	0.9999
XP 750387.1	Aspergillus fumigatus Af293	RNA exonuclease II1 subunit C11, putative	2	0.298141	0.394063	**1.3**	0.026973	0.099229	**0.5**	0.031810	0.344784	**2.5**	0.552184	0.915205	**1.1**	1.37E+04	2.19E+04	1.04E+04	1.76E+04	1.77E+04	2.33E+04	4.40E+04	4.13E+04	2.54E+04	1.40E+04	2.01E+04	1.94E+04	3	3	3	0.9861
XP 754574.1	Aspergillus fumigatus Af293	conserved hypothetical protein	3	0.060325	0.108699	**2.6**	0.002102	0.055680	**0.4**	0.077698	0.396006	**2.4**	0.000392	0.635000	**2.6**	2.40E+04	4.65E+04	1.32E+04	5.71E+04	6.94E+04	6.51E+04	7.42E+04	5.62E+04	5.17E+04	2.37E+04	2.19E+04	2.75E+04	21	21	21	1
XP 753396.1	Aspergillus fumigatus Af293	U6 small nuclear ribonucleoprotein (Lsm31, out	3	0.440265	0.569818	**1.7**	0.167623	0.282670	**0.5**	0.066066	0.381655	**2.2**	0.540760	0.914137	**1.6**	2.07E+04	2.03E+04	5.25E+04	7.25E+04	8.23E+04	1.70E+04	5.86E+04	6.96E+04	5.95E+04	1.66E+04	6.96E+04	2.31E+04	22	22	22	1
XP 750161.1	Aspergillus fumigatus Af293	coenzyme A transferase, putative	8	0.037411	0.076848	**1.7**	0.653907	0.789422	**0.7**	0.268297	0.591121	**2.2**	0.162553	0.758310	**2.1**	3.12E+04	1.22E+04	4.57E+04	9.10E+04	1.29E+05	7.37E+04	1.06E+05	7.27E+04	2.31E+04	2.42E+04	1.04E+05	2.74E+04	18	18	25	1
XP 747899.1	Aspergillus fumigatus Af293	nuclease RNAse III, putative	5	0.440847	0.570370	**1.2**	0.001131	0.042150	**0.3**	0.029533	0.357688	**2.1**	0.016269	0.706051	**2.0**	1.97E+04	3.12E+04	1.67E+04	2.04E+04	2.64E+04	3.60E+04	5.03E+04	5.62E+04	3.58E+04	1.51E+04	1.29E+04	1.21E+04	13	13	13	1
XP 753311.1	Aspergillus fumigatus Af293	conserved hypothetical protein	2	0.807675	0.887381	**1.0**	0.959783	0.142064	**0.5**	0.019007	0.344516	**2.1**	0.771310	0.969384	**0.9**	1.68E+04	1.85E+04	1.81E+04	1.77E+04	1.42E+04	2.00E+04	4.96E+04	4.18E+04	2.58E+04	1.27E+04	2.15E+04	2.31E+04	22	22	22	0.9991
XP 752750.1	Aspergillus fumigatus Af293	MFS multidrug transporter, putative	4	0.435450	0.564395	**1.6**	0.047589	0.129058	**1.0**	0.102780	0.430539	**2.1**	0.119908	0.709719	**0.4**	1.13E+04	2.68E+04	1.21E+04	1.67E+04	6.07E+04	1.45E+04	4.46E+04	2.14E+04	3.57E+04	6.25E+04	5.70E+04	6.14E+04	21	21	21	1
XP 753244.1	Aspergillus fumigatus Af293	ostwidemeiation factor subunit Cstf64, putative	2	0.515290	0.650073	**1.3**	0.668858	0.795706	**0.8**	0.011119	0.306764	**2.0**	0.817269	0.976055	**0.8**	1.78E+04	2.76E+04	2.76E+04	1.75E+04	6.03E+04	2.93E+04	4.36E+04	5.36E+04	4.83E+04	1.18E+04	6.50E+04	6.63E+04	13	13	13	0.9981
XP 753316.2	Aspergillus fumigatus Af293	BRCT domain protein	5	0.117924	0.180402	**0.3**	0.001540	0.052126	**0.3**	0.303810	0.609742	**2.0**	0.066919	0.662976	**0.5**	9.97E+04	1.45E+04	6.72E+04	1.99E+04	9.48E+03	1.23E+04	9.62E+04	1.12E+05	7.52E+04	3.20E+04	2.17E+04	2.20E+04	6	6	6	1
XP 750539.1	Aspergillus fumigatus Af293	heat shock protein Hsp30-like, putative	5	0.003077	0.037607	**2.8**	0.265323	0.395628	**1.7**	0.138343	0.472182	**2.0**	0.460175	0.886758	**0.8**	8.34E+03	1.21E+04	1.43E+04	3.24E+04	3.00E+04	1.27E+04	3.42E+04	2.88E+04	1.15E+04	2.47E+04	4.65E+04	4.64E+04	46	46	46	1
XP 753538.1	Aspergillus fumigatus Af293	DUF775 domain protein	6	0.230454	0.313026	**1.4**	0.031955	0.078403	**0.5**	0.056219	0.385139	**2.0**	0.065574	0.667294	**1.3**	3.02E+04	1.84E+04	2.19E+04	2.20E+04	2.34E+04	2.14E+04	3.78E+04	3.33E+04	2.55E+04	1.33E+04	1.69E+04	1.99E+04	11	11	11	1
XP 748111.1	Aspergillus fumigatus Af293	alpha/beta hydrolase, putative	5	0.934089	0.962975	**1.1**	0.035544	0.112841	**0.3**	0.199855	0.538364	**1.9**	0.465237	0.885753	**1.7**	1.60E+04	5.95E+04	4.52E+04	6.25E+04	1.26E+04	6.46E+04	7.24E+04	7.91E+04	5.17E+04	1.61E+04	1.62E+04	4.28E+04	15	15	15	1
XP 754599.1	Aspergillus fumigatus Af293	conserved hypothetical protein	2	0.000505	0.034954	**1.0**	0.916684	0.952408	**1.1**	0.095508	0.421193	**1.9**	0.105572	0.711281	**2.1**	2.21E+04	2.00E+04	1.94E+04	8.48E+04	1.38E+05	9.18E+04	2.19E+04	4.67E+04	5.68E+04	2.18E+04	8.74E+04	3.60E+04	5	5	5	0.999
XP 750799.1	Aspergillus fumigatus Af293	MFS multidrug transporter, putative	3	0.057046	0.104668	**1.6**	0.004605	0.055074	**0.5**	0.002418	0.317655	**1.9**	0.036525	0.719841	**1.9**	2.17E+04	2.14E+04	2.79E+04	3.66E+04	2.98E+04	5.28E+04	4.61E+04	4.46E+04	4.13E+04	2.13E+04	1.53E+04	2.41E+04	36	36	36	1
XP 747636.1	Aspergillus fumigatus Af293	mitochondrion biogenesis protein Mtm1, puta	5	0.994650	0.996430	**1.0**	0.018440	0.081107	**0.7**	0.198085	0.531380	**1.9**	0.630278	0.937596	**0.7**	1.74E+04	5.68E+04	5.95E+04	7.11E+04	1.28E+04	6.58E+04	6.79E+04	8.39E+04	6.83E+04	5.79E+04	5.09E+04	4.88E+04	27	27	27	1
XP 751179.1	Aspergillus fumigatus Af293	AP-3 adaptor complex subunit siema, putative	2	0.246819	0.332739	**1.4**	0.167043	0.282174	**0.7**	0.041144	0.360368	**1.8**	0.789232	0.969762	**1.1**	1.45E+04	2.23E+04	2.73E+04	2.17E+04	3.06E+04	1.42E+04	3.31E+04	4.29E+04	3.75E+04	2.95E+04	1.81E+04	3.47E+04	20	20	20	0.9991
XP 752937.1	Aspergillus fumigatus Af293	anaphase-promotine complex component Cut3	2	0.864084	0.922714	**1.1**	0.424700	0.580784	**0.7**	0.065831	0.381279	**0.5**	0.044183	0.677050	**3.3**	9.01E+04	1.91E+04	5.11E+04	4.88E+04	9.47E+04	4.85E+04	1.92E+04	2.00E+04	2.30E+04	1.22E+04	1.15E+04	3.67E+04	6	6	6	0.98
XP 750809.1	Aspergillus fumigatus Af293	SIR2 family histone deacetylase, putative	2	0.145540	0.447952	**0.7**	0.313055	0.451383	**1.4**	0.016047	0.343465	**0.4**	0.846890	0.985074	**1.1**	2.82E+04	2.82E+04	3.80E+04	0.03E+04	1.08E+04	2.93E+04	1.05E+04	1.92E+04	1.28E+04	3.05E+04	1.28E+04	1.91E+04	12	12	12	0.9991
XP 754931.1	Aspergillus fumigatus Af293	conserved hypothetical protein	3	0.068164	0.117145	**1.7**	0.005231	0.053628	**2.9**	0.013992	0.335049	**0.4**	0.228884	0.762740	**1.3**	1.85E+04	4.09E+04	2.70E+04	4.84E+04	8.26E+04	5.18E+04	1.36E+04	1.26E+04	2.05E+04	4.90E+04	5.04E+04	3.47E+04	23	23	23	1
XP 747619.1	Aspergillus fumigatus Af293	ara-tRNA aracesuine protein, putative	3	0.670006	0.792401	**0.8**	0.511969	0.687926	**1.1**	0.043835	0.363970	**0.4**	0.224315	0.759374	**1.7**	5.29E+04	2.30E+04	5.61E+04	4.85E+04	4.56E+04	1.65E+04	1.73E+04	1.98E+04	1.38E+04	2.60E+04	1.77E+04	1.51E+04	16	16	16	0.9988
XP 751284.1	Aspergillus fumigatus Af293	universal stress protein family domain protein	6	0.193495	0.269456	**0.8**	0.002636	0.058769	**2.7**	0.005538	0.327803	**0.4**	0.093464	0.702388	**0.8**	3.48E+04	2.78E+04	2.46E+04	1.88E+04	2.81E+04	2.17E+04	8.52E+03	1.15E+04	1.39E+04	2.99E+04	2.76E+04	3.13E+04	6	6	6	1
XP 754410.1	Aspergillus fumigatus Af293	domain Arc1 p20 subunit	2	0.090420	0.147485	**0.6**	0.554979	0.706184	**1.2**	0.022022	0.347832	**0.4**	0.204529	0.758305	**1.5**	4.03E+04	3.65E+04	3.69E+04	2.48E+04	3.41E+04	1.76E+04	1.23E+04	9.09E+03	2.32E+04	1.44E+04	1.44E+04	2.32E+04	18	18	18	0.9999
XP 754159.1	Aspergillus fumigatus Af293	hypothetical protein AFUA_3G14665	2	0.005557	0.039785	**0.3**	0.848240	0.914295	**1.1**	0.017233	0.345254	**0.3**	0.365871	0.838958	**0.8**	3.97E+04	4.04E+04	7.98E+04	1.50E+04	1.44E+04	1.37E+04	1.46E+04	1.31E+04	2.29E+04	2.41E+04	1.39E+04	1.50E+04	5	5	5	0.9991
XP 748741.1	Aspergillus fumigatus Af293	lipase/lanine esterase, putative	4	0.458457	0.590434	**0.6**	0.416348	0.571764	**1.8**	0.023467	0.348920	**0.3**	0.985386	0.996315	**1.0**	5.38E+04	6.44E+04	5.98E+04	6.39E+04	6.95E+04	8.88E+03	1.19E+04	3.46E+04	1.65E+04	5.38E+04	6.15E+04	1.13E+04	21	21	21	0.9992
XP 747964.2	Aspergillus fumigatus Af293	hah-affinite iron transporter FtrA	3	0.114749	0.176593	**0.4**	0.051397	0.132009	**2.7**	0.032120	0.350215	**0.3**	0.171341	0.769127	**0.5**	7.21E+04	8.02E+04	6.27E+04	1.57E+04	6.96E+04	1.99E+04	4.41E+04	1.88E+04	1.35E+04	7.42E+04	5.29E+04	5.87E+04	24	24	24	1
XP 752628.1	Aspergillus fumigatus Af293	hypothetical protein AFUA_1G12580	2	0.649579	0.774675	**1.1**	0.041486	0.122773	**4.3**	0.072200	0.394203	**0.3**	0.359781	0.836023	**0.8**	1.04E+05	7.54E+04	6.95E+04	7.63E+04	1.13E+05	8.13E+04	2.14E+04	1.19E+04	6.03E+04	1.11E+05	8.33E+04	1.35E+05	25	25	25	0.9991
XP 755960.1	Aspergillus fumigatus Af293	conserved hypothetical protein	3	0.227740	0.311119	**1.1**	0.047610	0.128925	**3.9**	0.056554	0.381742	**0.3**	0.942358	0.993612	**1.0**	1.08E+05	9.84E+04	1.03E+05	1.16E+05	1.32E+05	1.01E+05	1.98E+04	1.78E+04	7.58E+04	1.01E+05	1.04E+05	1.53E+05	24	24	24	0.999
XP 747782.1	Aspergillus fumigatus Af293	chitin synthase activator (Chs3), putative	5	0.116499	0.179011	**0.3**	0.142566	0.248005	**1.5**	0.000745	0.387111	**0.1**	0.768860	0.965676	**1.2**	1.34E+05	1.07E+05	8.50E+04	9.90E+04	2.03E+04	1.07E+04	1.12E+04	1.65E+04	1.95E+04	2.04E+04	2.92E+04	1.90E+04	7	7	7	1